AIP Publishing

This manuscript was accepted by Renewable Sustainable Energy. Click here to see the version of record.

Comparison of Cross-flow Turbine Performance under Torque-Regulated and Speed-Regulated Control

Brian Polagye,[1] Ben Strom,[1] Hannah Ross,[1] Dominic Forbush,[1] and Robert J. Cavagnaro[2]

[1)]*Department of Mechanical Engineering, University of Washington*

[2)]*Applied Physics Laboratory, University of Washington*

(Dated: 17 July 2019)

When experimentally evaluating the performance of a wind or water current turbine, one must impose a regulating torque on the turbine rotor by electrical or mechanical means. Some options limit this controlling torque to a purely resistive quantity, while servomotors and stepper motors allow torque to be applied in the direction of turbine rotation. Any control mode that results in net positive power for a turbine may be of interest for energy harvesting, and all of these are net "fluid-driven". Here, we present experiments that characterize the power, torque, and force coefficients of a cross-flow turbine operated at a constant rotational speed or under a constant imposed control torque. Time- and phase-average performance coefficients are largely equivalent for the two strategies, though torque-regulated control is restricted to a narrower range of rotational speeds and the two strategies result in slightly different blade kinematics.

ACCEPTED MANUSCRIPT

AIP Publishing

This manuscript was accepted by Renewable Sustainable Energy. Click here to see the version of record.

I. INTRODUCTION

In operational settings, wind or water current turbines use an electro-mechanical power take-off to convert rotational motion into electricity. In laboratory experiments, an equivalent power take-off is required. Researchers have used a variety of options, including mechanical or electrical friction brakes[1–5], miniature generators[6], stepper motors[7,8], and servomotors[9,10]. Mechanical and electrical friction brakes can only apply a control torque that opposes turbine rotation, while stepper motors and servomotors can apply a control torque that either acts in opposition to or in the same direction as turbine rotation. If the control torque is in the direction of rotation, this can give the impression that such motors inflate experimentally reported power output because the turbine is "motor-driven" rather than "fluid-driven". We note that the electro-mechanical conversion efficiency of stepper motors and servomotors is generally too low for commercial applications. However, as servomotors are topologically indistinct from permanent magnet generators, they are effective at emulating the dynamics of high-efficiency components.

Araya and Dabiri[3] studied the differences between wakes produced by a cross-flow turbine under "motor-driven" and "fluid-driven" operation using either a mechanical vise to impose a relatively constant control torque or a DC motor to impose a relatively constant rotational speed. They showed that, when the turbine was motored at higher rotational rates than could be achieved by resistive control torque, the turbine wake is significantly altered. However, at rotational rates accessible by either control mode, turbine performance was equivalent within the bounds of experimental uncertainty.

Here, we demonstrate that any differences arising between experiments with "motor-driven" or "fluid-driven" turbines are a consequence of differential hydrodynamics and blade kinematics, provided that net positive mechanical power (averaged over individual rotations) is produced by the turbine rotor. We focus on cross-flow (i.e., "vertical-axis") turbines, which have inherently unsteady dynamics, even in uniform inflow. The considerations presented in this paper can be extended to periodic aspects of axial-flow (i.e., "horizontal-axis") turbines, such as vertical shear, active blade pitch, and tower shadows. Similarly, while these experiments describe a water current turbine, results are transferable to wind turbines.

ACCEPTED MANUSCRIPT

AIP Publishing

This manuscript was accepted by Renewable Sustainable Energy. Click here to see the version of record.

II. BACKGROUND

The temporal evolution of rotational speed for a cross-flow turbine is described by Newton's second law for rotation

$$\frac{d\omega}{dt} = \dot{\omega} = \frac{Q_h - Q_c}{J} \tag{1}$$

where ω is the rotational speed of the turbine, t is time, J is the rotational moment of inertia of the turbine and power train, Q_h is the net hydrodynamic torque produced by the rotor (torque from blades, less opposition from fluid drag on rotating components), and Q_c is the electrical or mechanical control torque imposed on the rotor. The latter includes torque from a motor or brake, as well as any bearing friction. The product of J and rotational acceleration can also be conceived of as an "inertial torque".

If Q_c is regulated to match Q_h, then the rotational speed remains approximately constant. For the purposes of this paper, this control strategy is termed "speed-regulated control". If a constant, oppositional Q_c is imposed, then rotational speed can vary in time and, for the purposes of this paper, this control strategy is termed "torque-regulated control". In either case, torque is the control variable, but the controller objective differs. If Q_c varies with azimuthal position, such that neither rotational speed nor control torque is held constant, this is a form of "intracycle" control which, when optimized, has been shown to substantially increase net power output[10] by utilizing kinematic and hydrodynamic mechanisms.

If a turbine is tested according to the arrangement shown in Fig. 1, then the control torque applied to the turbine is equal to the sum of the torques measured by each load cell

$$Q_c = Q_m + Q_b \tag{2}$$

where Q_m is the torque applied by the servomotor and Q_b is the torque applied by the bearing. Consequently, the time-varying hydrodynamic torque may be calculated from measurements as

$$Q_h(t) = J\dot{\omega}(t) + Q_c(t). \tag{3}$$

The instantaneous hydrodynamic power, $P_h(t)$, is

$$P_h(t) = Q_h(t)\,\omega(t). \tag{4}$$

This quantity describes the hydrodynamic energy harvesting capability of a turbine (i.e., the conversion from hydrodynamic to mechanical energy), independent of losses in the secondary conversion from mechanical to electrical energy in the power take-off. Hydrodynamic power can be

ACCEPTED MANUSCRIPT

AIP Publishing

This manuscript was accepted by Renewable Sustainable Energy. Click here to see the version of record.

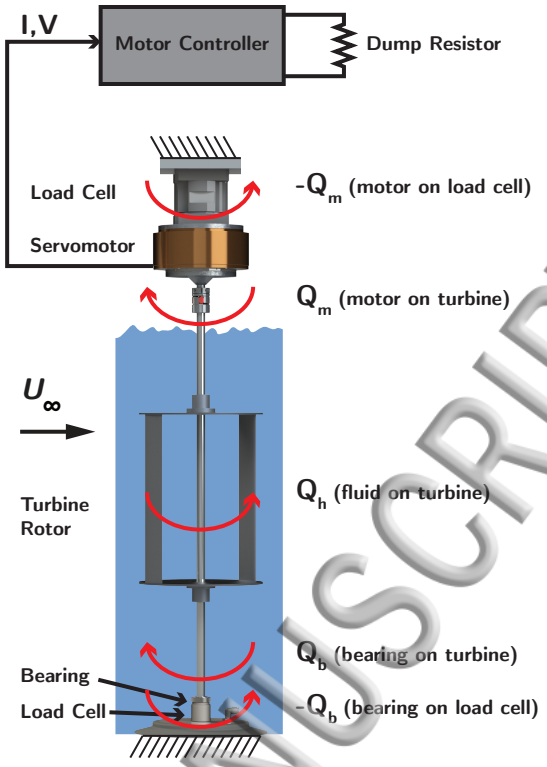


FIG. 1. Schematic of cross-flow turbine testing apparatus with applied and measured torques indicated.

expressed as a non-dimensional hydrodynamic power coefficient, $C_{P,h}(t)$, as

$$C_{P,h}(t) = \frac{Q_h(t)\,\omega(t)}{\frac{1}{2}\rho A U_o(t)^3} \tag{5}$$

where ρ is the density of water, A is the projected rotor area, and U_o is the undisturbed inflow velocity.

If $C_{P,h}(t) > 0$, mechanical power is being generated by the turbine rotor. Under speed-regulated control, this power is transferred to the power take-off where it is either dissipated by friction or converted to electricity. Under torque-regulated control, the imbalance between hydrodynamic and control torque can also accelerate the turbine, converting mechanical power to rotational kinetic power. Conversely, if $C_{P,h}(t) < 0$, mechanical power is being consumed by the turbine rotor. Under speed-regulated control, the power take-off must transfer mechanical power to the turbine to offset hydrodynamic power consumption. Under torque-regulated control, since only an oppositional torque can be applied to the turbine, hydrodynamic power consumption must be balanced by decelerating the turbine rotor and harvesting rotational kinetic power.

It is important to note that no electrical power terms appear in this definition of $C_{P,h}(t)$ (Eq. 5). The only aspect of the power take-off that influences turbine dynamics is whether the power take-

ACCEPTED MANUSCRIPT

AIP Publishing

This manuscript was accepted by Renewable Sustainable Energy. Click here to see the version of record.

off is capable of applying torque in the direction of rotation or only in opposition to rotation. For example, if a mechanical friction brake, servomotor, and particle brake apply the same $Q_c(t)$, the resulting $Q_h(t)$ will be identical, even though the particle brake consumes electrical power to resist the turbine rotation, the servomotor can produce electrical power that is dissipated by a dump resistor, and the friction brake neither produces nor consumes electrical power. We further note that, even when $C_{P,h}(t) > 0$, a servomotor may still be consuming electrical power, since the power generated may be less than internal losses.

The turbine's rotational speed may be non-dimensionalized as a tip-speed ratio, $\lambda(t)$, defined as

$$\lambda(t) = \frac{R\omega(t)}{U_o(t)} \tag{6}$$

where R is the turbine radius. Further, the hydrodynamic torque coefficient, $C_{Q,h}$, is defined as

$$C_{Q,h}(t) = \frac{Q_h(t)}{\frac{1}{2}\rho A R U_o(t)^2} \tag{7}$$

and, by dividing Eq. 5 by Eq. 7, it can be shown that these quantities are related as

$$\lambda(t) = \frac{C_{P,h}(t)}{C_{Q,h}(t)}. \tag{8}$$

In the literature, it is common to express the characteristic power performance of a turbine in terms of the relationship between the time-averages of $C_{P,h}$ and λ as

$$\langle C_{P,h} \rangle = \langle C_{P,h}(t) \rangle = \left\langle \frac{Q_h(t)\,\omega(t)}{\frac{1}{2}\rho A U_o(t)^3} \right\rangle \tag{9}$$

$$\langle \lambda \rangle = \langle \lambda(t) \rangle = \left\langle \frac{R\omega(t)}{U_o(t)} \right\rangle \tag{10}$$

These average quantities can be expressed for all rotations at a control set point (e.g., constant ω) or as an average over a single rotation.

However, Eq. 1 allows for instantaneous differences between $Q_h(t)$ and $Q_c(t)$ such that the hydrodynamic power produced by the turbine may instantaneously deviate from the shaft power available at the power take-off. Therefore, one could alternatively define a control power coefficient, $C_{P,c}$, in terms of the control torque as

$$C_{P,c}(t) = \frac{Q_c(t)\,\omega(t)}{\frac{1}{2}\rho A U_o(t)^3}. \tag{11}$$

ACCEPTED MANUSCRIPT

AIP Publishing

This manuscript was accepted by Renewable Sustainable Energy. Click here to see the version of record.

This distinction is not generally noted in the literature and either definition yields approximately the same time-average result. As proved in Appendix A, even for control strategies with angular acceleration (i.e., $\dot{\omega}(\theta) \neq 0$), if $\omega(\theta)$ is periodic over a single rotation, then the integral of the inertial torque (i.e., $J\dot{\omega}$) over a single rotation must be zero, and the cyclic integral of Q_c is equal to the cyclic integral of Q_h. This is strictly true under speed-regulated control, such that $\langle C_{P,h} \rangle = \langle C_{P,c} \rangle$, but is only approximate under torque-regulated control because $\omega(\theta)$ is not guaranteed to be periodic with rotation. As shown in Appendix A, the error associated with this approximation can be significant at some tip-speed ratios, such that it is most accurate to characterize time-average turbine performance in terms of $\langle C_{P,h} \rangle$.

Further, the distinction between hydrodynamic and control torque is significant when considering phase-average performance (i.e., average performance as a function of azimuthal position). Using the hydrodynamic power coefficient as an example, the conditional average may either be expressed in absolute terms as

$$C_{P,h}(\theta) = \langle C_{P,h}(t) \,|\, \theta \rangle \tag{12}$$

or in relative terms as

$$\Delta C_{P,h}(\theta) = C_{P,h}(\theta) - \langle C_{P,h} \rangle. \tag{13}$$

If experimental data are collected in a phase-locked manner (i.e., torque and rotation rate sampled at discrete θ), then these quantities may be calculated directly. On the other hand, if experimental data are collected at a constant acquisition rate in time, then the conditional mean must be calculated for populations drawn from relatively narrow azimuthal ranges.

Structural loads on the turbine may be non-dimensionalized as

$$C_T(t) = \frac{T(t)}{\frac{1}{2}\rho A U_o(t)^2} \tag{14}$$

$$C_L(t) = \frac{L(t)}{\frac{1}{2}\rho A U_o(t)^2} \tag{15}$$

where T is the thrust force developed in the direction of the inflow and L is the lateral force developed perpendicular to the inflow. As for the power and torque coefficients, these force coefficients may be time- or phase-averaged.

The blade kinematics can provide insight into variations in phase-average performance. The nominal angle of attack, $\alpha_n(t)$ encountered by the rotating blade of a cross-flow turbine may be

ACCEPTED MANUSCRIPT

AIP Publishing

This manuscript was accepted by Renewable Sustainable Energy. Click here to see the version of record.

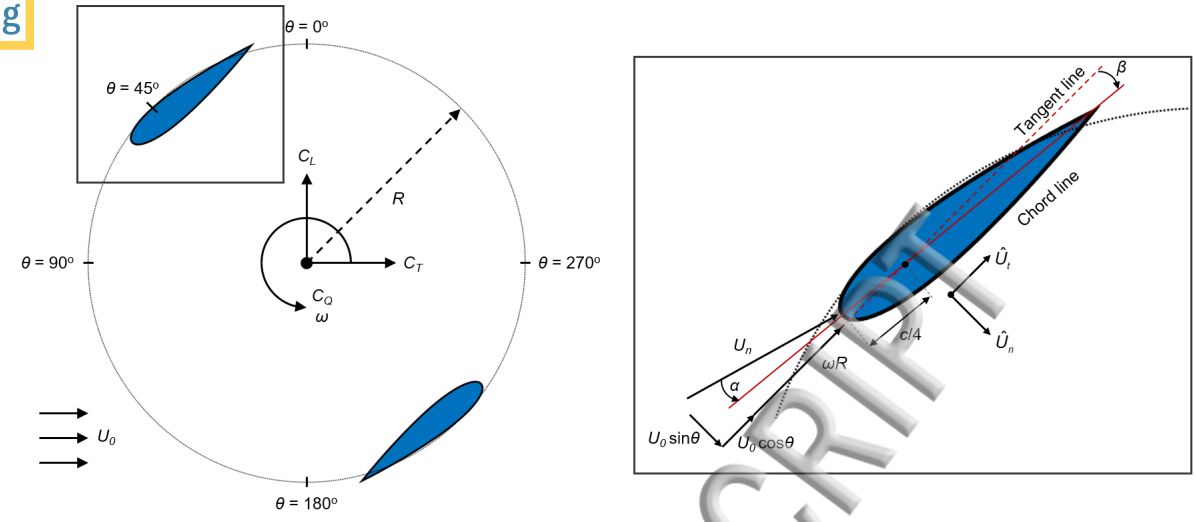


FIG. 2. Angular position, torque, and force definitions. The right-hand panel shows the details of the nominal velocity, nominal angle of attack, and preset pitch angle. The unit tangential vector is defined as parallel to the tangent line and the unit normal vector is defined perpendicular to this.

approximated as

$$\alpha_n(t) = -\arctan\left(\frac{\sin\theta(t)}{\lambda(t)+\cos\theta(t)}\right)+\beta(t) \tag{16}$$

where $\beta(t)$ is the blade pitch angle (Fig. 2). For cross-flow turbines with fixed pitch, $\beta(t)$ is a constant. Eq. 16 describes a "nominal", rather than true, angle of attack because it neglects induction in the along- and across-stream directions. While analytical solutions exist for these factors[11], they have been shown to poorly predict performance of cross-flow turbines with relatively high solidity[12]. Further, the true angle of attack is difficult to uniquely specify, even with complete knowledge of the flow field[13]. As shown by Samoano and Huera-Huarte[14], an assumption of negligible induction is invalid for the downstream portion of the stroke ($180^o \leq \theta \leq 360^o$, Fig. 2), where the blades pass through their own wake. However, Eq. 16 can provide semi-quantitative information for the upstream portion of the stroke. With the same assumptions, the normalized nominal relative velocity, $U_n^*(t)$, can be expressed as

$$U_n^*(t) = \frac{U_n(t)}{U_o(t)} = \sqrt{\lambda(t)^2 + 2\lambda(t)cos(\theta)+1} \tag{17}$$

where $U_n(t)$ is the vector sum of the inflow velocity and blade velocity, as shown in Fig. 2.

ACCEPTED MANUSCRIPT

AIP Publishing

This manuscript was accepted by Renewable Sustainable Energy. Click here to see the version of record.

III. METHODS

Our experiments utilized the apparatus shown schematically in Fig. 1 and as implemented experimentally in Fig. 3. The upper load cell was a 6-axis Mini45 (ATI Industrial Automation) and the lower load cell was a 6-axis Nano25 (ATI Industrial Automation). A servomotor (Yaskawa SGMCS-05B3C41) equipped with a 2^{18} count encoder regulated the turbine's rotation. The upper load cell was thermally isolated from the servomotor by ceramic stand-offs. Rotational speed, torque, and forces were acquired using National Instruments DAQs (2x model 6351) at a sampling rate of 1000 Hz. Inflow velocity was measured by an acoustic Doppler velocimeter (Nortek Vector) with a sample volume five rotor diameters upstream of the turbine at the vertical center plane. Velocity measurements were acquired at rate of 64 Hz and despiked using the method of Goring and Nikora[15]. Data collection and turbine control were implemented in Matlab and Simulink (Mathworks) using custom scripts.

As shown in Fig. 4, the turbine rotor had two straight blades with NACA 0018 profiles. The turbine's diameter, D, was 17.2 cm, its height, H, was 24.7 cm, and the blade chord length, c, was 4.06 cm. The blades were mounted at a 6^{o} preset pitch (leading edge rotated outward about the quarter-chord) and connected to the central drive shaft by a pair of foil-shaped struts (NACA 0016 profile with the same chord length as the blade). This configuration was semi-arbitrary (an experimental configuration used previously to study the influence of support structures on turbine performance[16]) and does not represent an optimal cross-flow geometry. A brief discussion of the nuanced influences of these geometric parameters is given in Appendix B.

The rotational moment of inertia was estimated experimentally as 0.0102 ± 0.0003 kg-m^2 by oscillatory rotation of the turbine in air. Under these conditions, "hydrodynamic" forces were negligible in comparison to in-water operation, and the turbine dynamics reduced to

$$\dot{\omega} = -\frac{Q_c}{J} \tag{18}$$

in which the rotational moment of inertia, J, was the only unknown quantity. J was estimated by a least-squares fit to data from a sinusoidally-varying rotational speed trajectory with constant amplitude. This procedure was repeated at different amplitudes and the mean of these cases taken as a best estimate for the rotational moment of inertia of the turbine and power take-off. We note that this procedure underestimates the rotational moment of inertia in water because it neglects added mass. However, were a similar experiment to evaluate added mass be conducted in water, a model for the hydrodynamic torque on an accelerating turbine would be required. In our view,

ACCEPTED MANUSCRIPT

AIP Publishing

This manuscript was accepted by Renewable Sustainable Energy. Click here to see the version of record.

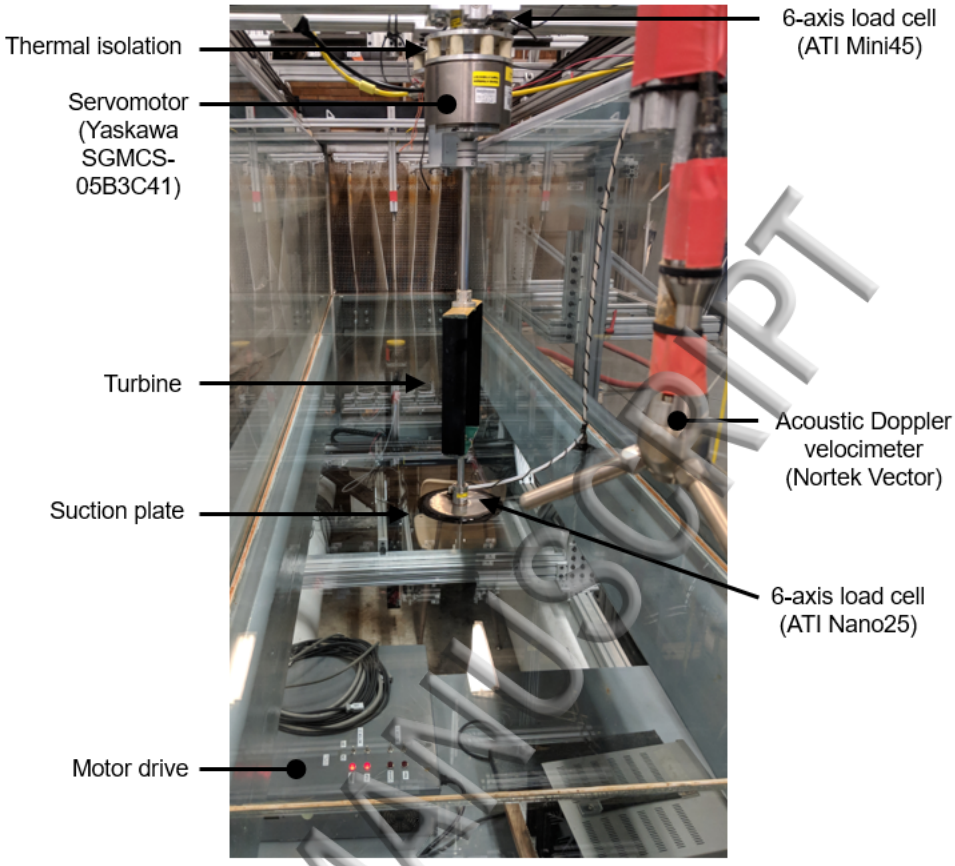


FIG. 3. Annotated picture of experimental setup. The flume has been drained for rotational moment of inertia estimation.

the approximation required for such a model (e.g., assuming that hydrodynamic torque is invariant with periodic acceleration about a mean rotational speed), would likely introduce greater uncertainty in the estimate for J than neglecting added mass, particularly given that, for this experiment, the servomotor contributes approximately $\frac{1}{2}J$.

Experiments were conducted in the Alice C. Tyler flume at the University of Washington. Inflow velocity was maintained at ~ 1 m/s, water depth at ~ 50 cm, and water temperature at 22 ^{o}C. During the experiments, turbulence intensity was ~ 2 %, the Froude number was 0.45, and the blockage ratio (turbine projected area relative to channel cross-section) was ~ 11 %. The latter neglects the area occupied by the support structure (e.g., turbine shaft, vacuum plate mounting) which was on the same order as channel cross-sectional area uncertainty from free surface variations around the turbine. No free surface deformation was observed as a consequence of energy extraction.

ACCEPTED MANUSCRIPT

This manuscript was accepted by Renewable Sustainable Energy. Click here to see the version of record.

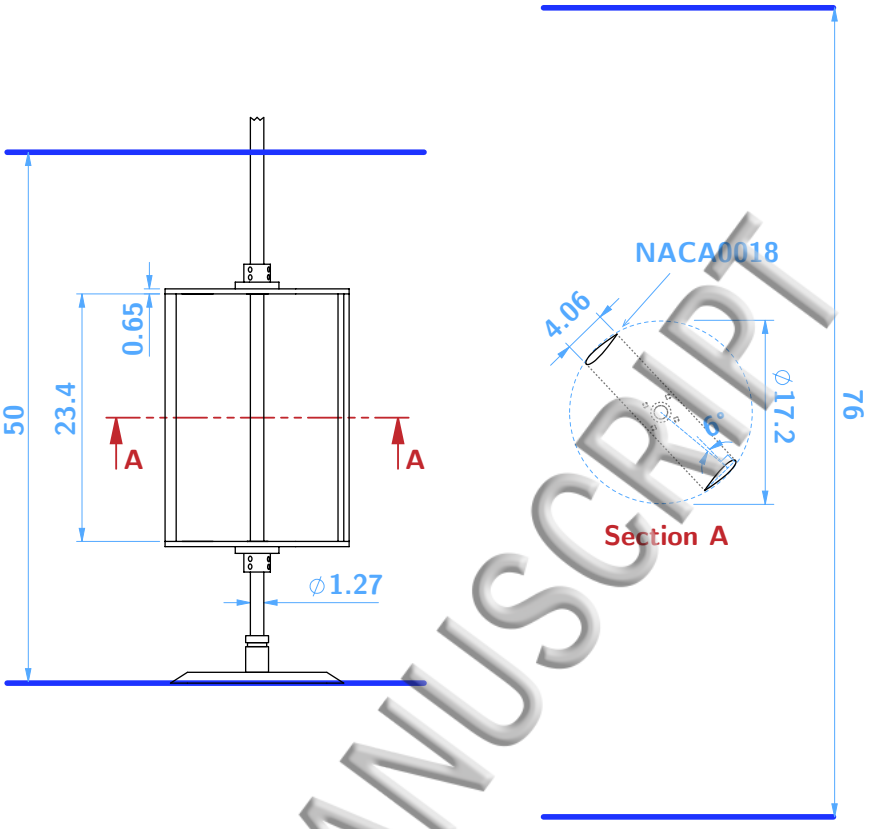


FIG. 4. Schematic drawing of cross-flow turbine with key dimensions given in cm. The left-hand figure is a cross-sectional view with the upper blue line denoting the nominal water surface. The right-hand figure is a plan view (i.e., top-down), with the blue lines denoting the flume side walls.

The Reynolds number was defined as

$$\mathrm{Re} = \frac{U_o D}{\nu} \tag{19}$$

where ν is the kinematic viscosity of water. For these experiments, $\mathrm{Re} = 1.8x10^5$. This means that the turbine was generally operating at a transitional Re[5,17]. Consequently, the "characteristic" non-dimensional performance curves presented here are specific to this Re.

Experiments assessed turbine performance under speed- or torque-regulated control. Under speed-regulated control, the servomotor drive was commanded to maintain a constant rotational speed, which was achieved internal to the drive with a feedback loop on encoder output. Under torque-regulated control, because the motor drive could not directly measure control torque, a proportional-integral feedback control loop was implemented in Matlab. The control loop input was torque measured by the load cells, in N-m, and the output was a command torque voltage signal sent from the DAQ to the motor drive. To reduce the effects of electromagnetic interference

ACCEPTED MANUSCRIPT

AIP Publishing

This manuscript was accepted by Renewable Sustainable Energy. Click here to see the version of record.

from the motor drive, measured torque was filtered using a low-pass, first-order Butterworth filter with a cut-off frequency of 1 Hz. In the proportional-integral feedback control loop, the error signal was the difference between the measured and specified control torque. The proportional gain was 10 V/N-m and integral gain was 35 V/N-m. This feedback arrangement resulted in more stable turbine operation than a constant, open-loop voltage command to the motor drive. For the experiments, the turbine was operated at a series of set points defined by either a constant rotational speed or constant control torque, with each set point maintained for 56.5 s. Between each set point, the turbine was allowed 5 s to equilibrate.

Because inflow velocity was measured upstream of the turbine, a time correction on U_o is required to calculate instantaneous coefficients. This was empirically estimated using the cross-correlation between low-pass filtered inflow velocity and hydrodynamic power, as described in Appendix C. Representative time-average performance at each control set point was taken as the mean of the instantaneous performance coefficients. The variability in time-average performance was quantified by the interquartile range (IQR) of coefficients averaged over a single rotation. For phase-average performance, a 4^o azimuthal range was used, and the mean and IQR calculated from the population of instantaneous coefficients within this range. Experimental repeatability is quantified for the time-average hydrodynamic power coefficient in Appendix D.

IV. RESULTS

As shown in Fig. 5, $\langle C_{P,h} \rangle$ and the interquartile range for individual revolutions are almost identical between the two control strategies in their common operating region. Operation under torque-regulated control produces a slightly higher $\langle C_{P,h} \rangle$, though the range of operable tip-speeds is more limited than when rotational speed is held constant. For rotational speeds where $\langle C_{P,h} \rangle < 0$, net power input is required to rotate the turbine. Otherwise, net power is produced. The highest possible steady-state rotational speed achievable under resistive control torque is referred to as the "freewheel" tip-speed ratio and corresponds to $\langle Q_h \rangle = 0$, since all hydrodynamic torque produced by the blades is dissipated by drag on the rotating components. As a consequence, at freewheel, $\langle Q_c \rangle = 0$ and no net power is delivered to the power take-off. This state is theoretically accessible through either resistive power take-offs or those that can impose a torque in the direction of turbine rotation (e.g., a servomotor). In practice, however, a resistive torque mechanism often imposes a small, uncontrollable torque associated with friction, such that $\langle Q_c \rangle > 0$, even without any control

ACCEPTED MANUSCRIPT

AIP Publishing

This manuscript was accepted by Renewable Sustainable Energy. Click here to see the version of record.

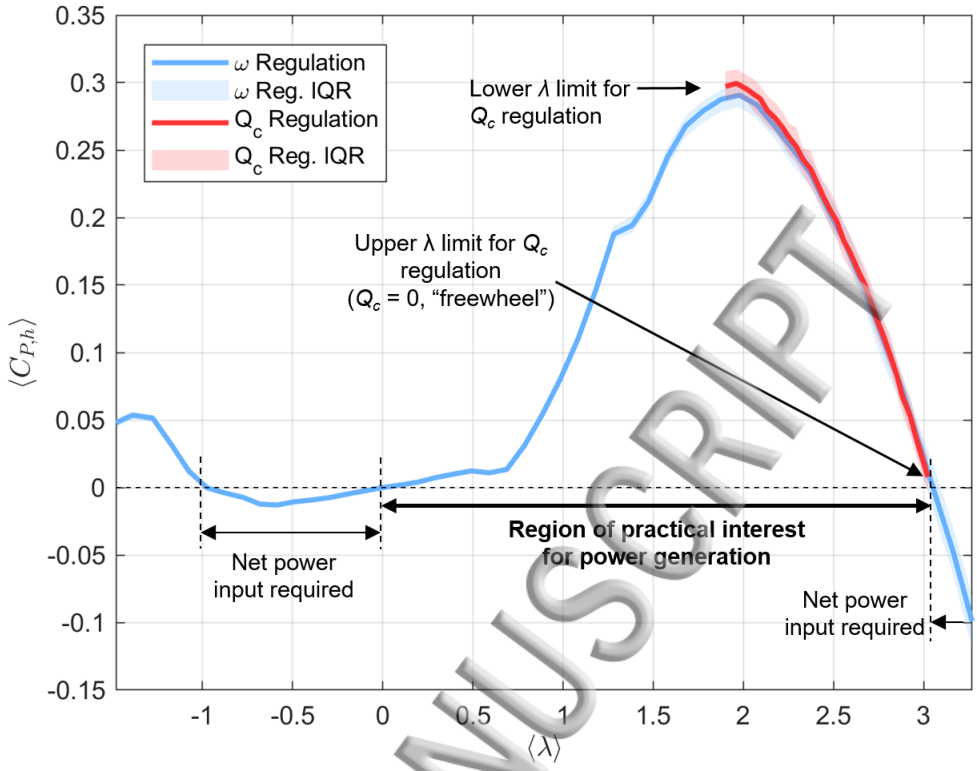


FIG. 5. Time-average hydrodynamic power as a function of tip-speed ratio under speed- and torque-regulated control.

actuation. The other end of the useful operating range corresponds to a nearly stopped turbine and is not accessible using a purely resistive power take-off. While not of practical interest, it is possible to produce power by rotating the turbine "backwards", such that the position of the leading and trailing edges of the blades are effectively reversed. Further discussion focuses on the region of practical interest for energy generation schemes.

As shown in Fig. 6b, the lowest achievable tip-speed ratio under torque-regulated control is close to the maximum value of the hydrodynamic torque coefficient. This is expected, because the maximum sustainable control torque cannot exceed the maximum achievable hydrodynamic torque[18]. If control torque is increased beyond this value, either through control actuation or reduction in inflow velocity due to turbulence, the turbine rotor will rapidly decelerate to a complete stop. In uniform inflow, it would be possible to reach the peak of the $\langle C_{Q,h} \rangle - \langle \lambda \rangle$ curve under torque-regulated control, but, due to turbulence, the range of operable tip-speed ratios is reduced.

The time-average thrust coefficient, $\langle C_T \rangle$ (Fig. 6c), increases monotonically with tip-speed ratio and is nearly independent of control strategy. The lateral force coefficient, $\langle C_L \rangle$ (Fig. 6d), is

ACCEPTED MANUSCRIPT

AIP Publishing

This manuscript was accepted by Renewable Sustainable Energy. Click here to see the version of record.

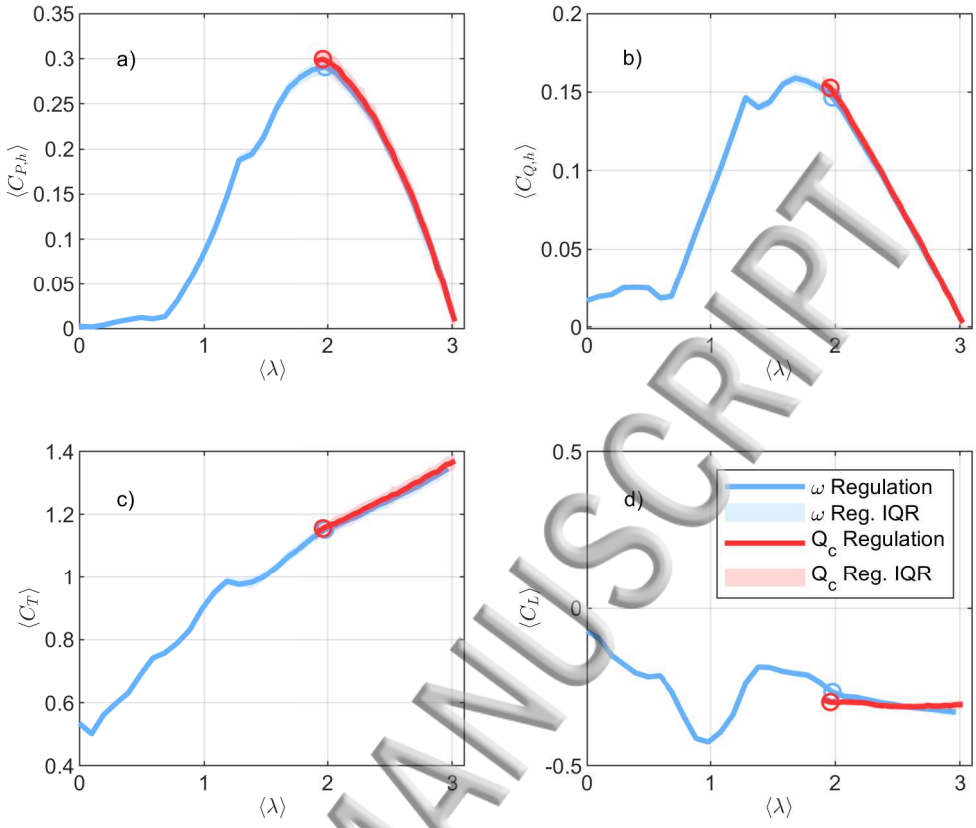


FIG. 6. Time-average turbine performance coefficients in region of practical interest for speed- and torque-regulated control for (a) hydrodynamic power coefficient, (b) hydrodynamic torque coefficient, (c) thrust, and (d) lateral force. Open circles denote the tip-speed ratio corresponding to the maximum power coefficient under torque-regulated control and the closest equivalent tip-speed ratio under speed-regulated control.

smaller, has less dependence on tip-speed ratio, and has a mild dependence on control strategy. Its direction is consistent with lift produced by circulation around a rotating cylinder[19] and as $\langle \lambda \rangle < 0$, $\langle C_L \rangle > 0$ (not shown). Unlike the thrust coefficient, there is a local extrema at the transition point from lift-based operation ($\langle \lambda \rangle > 1$) to drag-based operation ($0 \leq \langle \lambda \rangle \leq 1$). Finally, because thrust and lateral forces vary significantly with tip-speed ratio, experiments or simulations evaluating wake dynamics for cross-flow turbines should give consideration to where on the characteristic performance curve a turbine is operating.

Fig. 7 shows absolute, phase-average performance at the tip-speed ratio corresponding to max-

ACCEPTED MANUSCRIPT

AIP Publishing

This manuscript was accepted by Renewable Sustainable Energy. Click here to see the version of record.

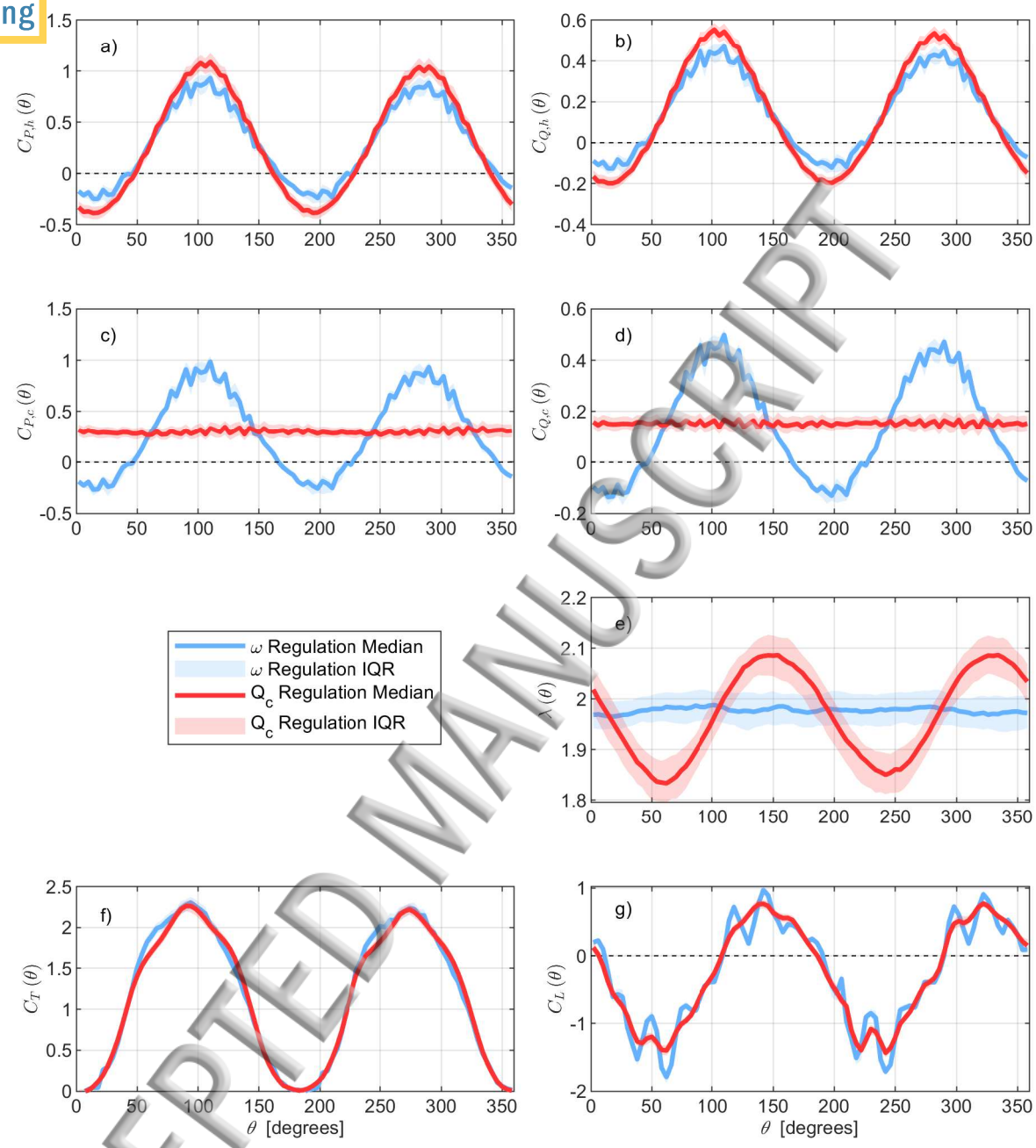


FIG. 7. Phase-average turbine performance coefficients at tip-speed ratio corresponding to the maximum power coefficient under torque-regulated control and the closest equivalent tip-speed ratio under speed-regulated control: (a) hydrodynamic power coefficient, (b) hydrodynamic torque coefficient, (c) control power coefficient, (d) control torque coefficient, (e) tip-speed ratio, (f) thrust coefficient, and (g) lateral force coefficient.

ACCEPTED MANUSCRIPT

AIP Publishing

This manuscript was accepted by Renewable Sustainable Energy. Click here to see the version of record.

imum $\langle C_{P,h} \rangle$ under torque-regulated control and the closest equivalent tip-speed ratio under speed-regulated control. As expected for a two-bladed turbine, twice-per-rotation periodicities are apparent under both control schemes. There are higher-frequency oscillations in C_Q and, consequently, C_P, which are likely an artifact of torsional resonance in the upper load cell. The phase-average force coefficients are nearly independent of control scheme (Fig. 7f,g), with the periodic maxima in along-stream forces leading the maxima in across-stream forces. Further, while the along-stream forces are unidirectional, the direction of the across-stream forces oscillates with azimuthal position. Therefore, while the net effect in the across-stream direction (Fig. 6d) is a force consistent with circulation around a cylinder, the time-varying hydrodynamics indicate that this force simply arises from the resultant lift and drag on the foil.

The tip-speed ratio, torque coefficients, and power coefficients depend strongly on the control objective. Phase-average variations in the tip-speed ratio (Fig. 7e) are negligible under speed-regulated control, though turbulence produces a range of λ for a given ω. Correspondingly, control torque (Fig. 7c) variations are negligible under torque-regulated control. However, regardless of control scheme, the hydrodynamic power and torque coefficients oscillate with azimuthal position (Fig. 7a,b) and both control schemes have phases where hydrodynamic power is consumed by the rotor. During these periods, under speed-regulated control, the servomotor applies a torque in the direction of rotation, while under torque-regulated control, the rotational kinetic power decreases.

As shown in Fig. 8, the similarity in hydrodynamic power between control schemes is consistent with the blade kinematics. Although the blade kinematics are only presented for the upstream sweep of a single blade, both blades contribute to the phase-average hydrodynamic power. However, because of the energy harvesting during the upstream sweep, the nominal relative velocity for the downstream blade is substantially reduced and its contribution to hydrodynamic power is likely limited. Under torque-regulated control, the nominal angle of attack trajectory (Fig. 8b) is slightly steeper and the normalized nominal relative velocity (Fig. 8c) is slightly higher for phases corresponding to maximum power generation, potentially explaining the slightly higher time-average $C_{P,h}$. Further, during maximum power generation, under both control schemes, the nominal angle of attack is much greater than the static stall angle[20]. This suggests that dynamic stall is maintaining a favorable lift-to-drag ratio at higher angles of attack[21] and/or induction (neglected in Eq. 16) is substantial. Because these experiments take place at a transitional Reynolds number, the variations in U_n^* likely have some effect on the hydrodynamic power coefficient variations between control schemes. For turbines with a lower rotational moment of inertia, there might

ACCEPTED MANUSCRIPT

AIP Publishing

This manuscript was accepted by Renewable Sustainable Energy. Click here to see the version of record.

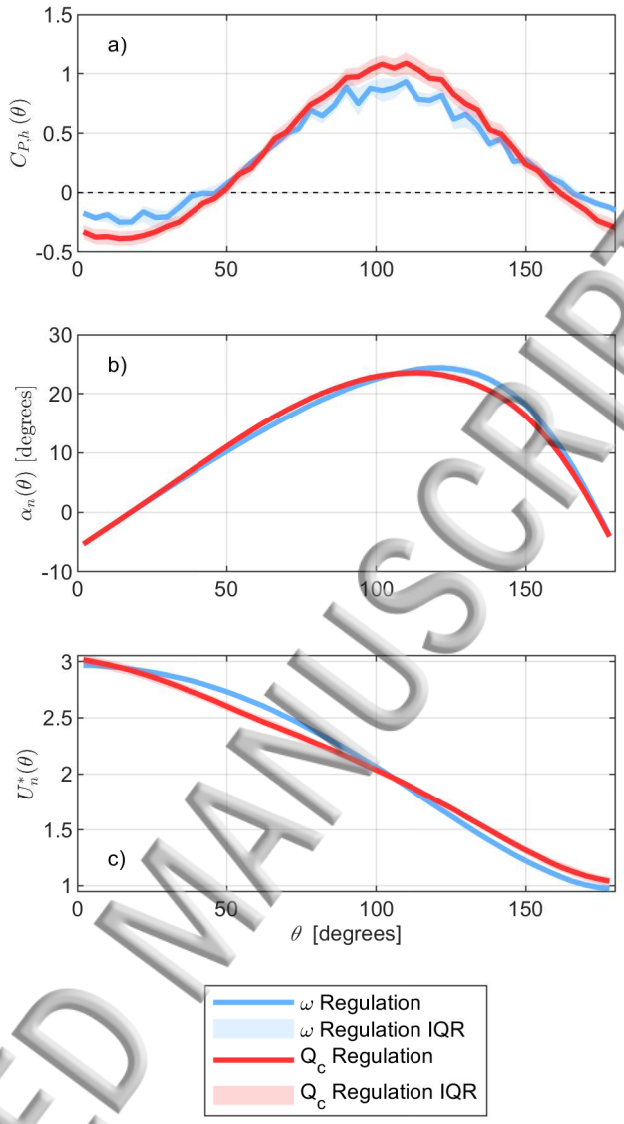


FIG. 8. Phase-average (a) hydrodynamic power coefficient, (b) nominal angle of attack, and (c) normalized nominal relative velocity at tip-speed ratio corresponding to the maximum power coefficient under torque-regulated control and the closest equivalent tip-speed ratio under speed-regulated control.

be more meaningful differences in the blade kinematics between control schemes and, therefore, the time-average hydrodynamic power coefficients.

We note that $C_{P,h}(\theta)$ exceeds unity for part of the cycle under torque-regulated control and, for both control schemes, $C_{P,h}(\theta)$ exceeds the time-average Betz limit[22]. Obviously, if $C_{P,h}(\theta) < \langle C_{P,h} \rangle$ for a subset of azimuthal positions, it must exceed $\langle C_{P,h} \rangle$ for others. However, because the turbine is operating in a confined flow and blockage corrections are not meaningful for phase-

ACCEPTED MANUSCRIPT

AIP Publishing

This manuscript was accepted by Renewable Sustainable Energy. Click here to see the version of record.

average performance, it is unknown if this is a consequence of blockage or a general feature of cross-flow turbine performance. In other words, is unclear whether a cross-flow turbine in unconfined flow can have a $C_{P,h}(\theta)$ that exceeds the Betz limit for some azimuthal positions, but $\langle C_{P,h} \rangle$ below the Betz limit. We are not aware of any investigation of this question in the archival literature, including simulations of cross-flow turbines with variable blade pitch[23,24].

As shown in Fig. 9, the trends in phase-average performance coefficients shown in Fig. 7 are robust over tip-speed ratios accessible by either control strategy. For speed-regulated control, as tip-speed ratio decreases, flow separation may occur earlier in rotation (as anticipated by Eq. 16) and, consequently, the phase-average maxima in the power and torque coefficients are shifted earlier in the cycle. Phase variations in along-stream and across-stream forces are more consistent over all tip-speed ratios. This suggests that phase variation in force coefficients primarily depends on turbine geometry.

V. DISCUSSION

A. Generalization to other Turbines and Settings

Here, we discuss how the laboratory results presented in Sec. IV could be affected by turbine scale and setting. For simplicity, we neglect the influence of the Reynolds number on performance coefficients, but note that as turbine scale increases, up to the limit of Reynolds independence, the maximum power coefficient increases[5,17]. This has implications for the time-average control torque coefficient in the following discussion.

It is instructive to consider the time scales present in the laboratory experiments. As shown in Appendix E, for our laboratory-scale turbine, the primary periodicity in turbine power output and loads is at the blade passage frequency (i.e., intracycle variability), which is approximately two orders of magnitude faster than the dominant energy-containing turbulence in the flume. Consequently, in our laboratory experiments, turbulence interacts with the rotor as an "engulfing gust" that is equivalent to a relatively slow time variation in the mean flow (i.e., within a single rotation, the inflow velocity is approximately constant). For a given tip-speed ratio, the blade passage frequency is inversely proportional to the turbine's geometric scale. Consequently, as turbine scale increases and/or a turbine is operated in an environment with energy-containing turbulence at higher frequencies, turbulence could act within a single rotation. This would likely increase

ACCEPTED MANUSCRIPT

AIP Publishing

This manuscript was accepted by Renewable Sustainable Energy. Click here to see the version of record.

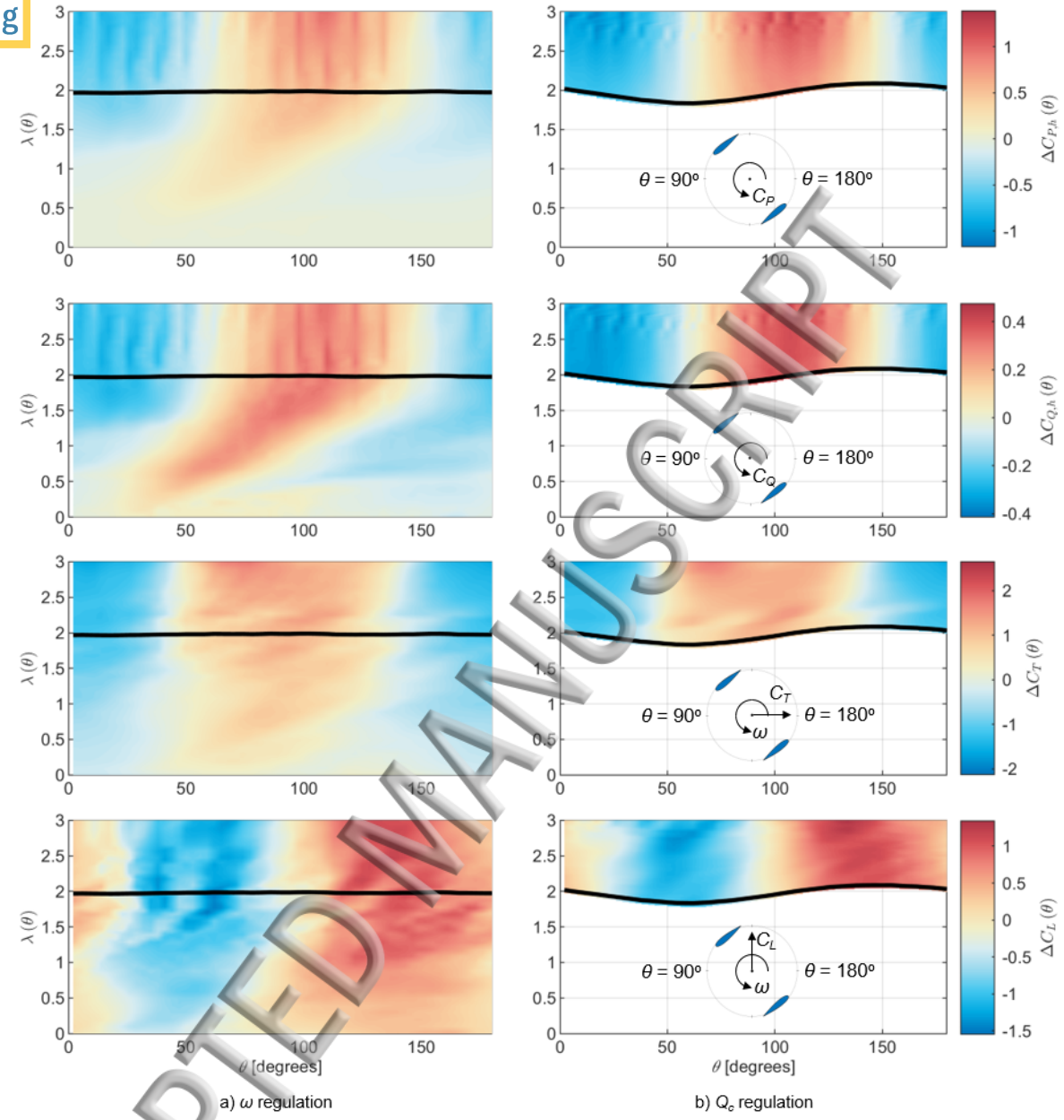


FIG. 9. Phase-average turbine performance variations in region of practical interest for energy generation under a) speed-regulated control and b) torque-regulated control. From top to bottom: relative hydrodynamic power coefficient, hydrodynamic torque coefficient, thrust coefficient, and lateral force coefficient. Solid black lines denote the cases shown in Fig. 7.

cycle-to-cycle variability in turbine performance.

Along these lines, Tobin et al.[6] introduce the concept of an inertial time scale, t_i, defined as

$$t_i = \frac{J\omega}{2Q_c}. \tag{20}$$

ACCEPTED MANUSCRIPT

AIP Publishing

This manuscript was accepted by Renewable Sustainable Energy. Click here to see the version of record.

This can be used to describe the effect of turbulence on turbine power as a decaying impulse-response. If ω and Q_c are taken as the time-average value for a control set point and noting that $A = 2RH$, then Q_c can be expressed as

$$Q_c = \rho U_o^2 R^2 H \langle C_{Q,c} \rangle, \tag{21}$$

where U_o is the time-average velocity. The rotation rate can be similarly expressed as

$$\omega = \frac{\langle \lambda \rangle U_o}{R}. \tag{22}$$

If the rotational moment of inertia is dominated by the turbine blades,

$$J = \frac{1}{2} R^2 m_b \tag{23}$$

where m_b is the mass of the turbine blades and

$$m_b = NHA_b \rho_b \tag{24}$$

where N is the number of blades, A_b is the blade cross-sectional area, and ρ_b is the blade density. A_b can be expressed as

$$A_b = cL \tag{25}$$

where L is the mean blade thickness. Substituting Eq. 25 and Eq. 24 into Eq. 26

$$J = \frac{1}{2} R^2 NHcL\rho_b. \tag{26}$$

By substituting Eqs. 21, 22, and 26 into Eq. 20, t_i can be expressed as

$$t_i = \frac{1}{4} N \frac{c}{R} \frac{L}{U_o} \frac{\rho}{\rho_b} \frac{\langle \lambda \rangle}{\langle C_{Q,c} \rangle}. \tag{27}$$

This allows us to evaluate how t_i would vary between a laboratory-scale turbine, l, and a larger turbine in the field, f. If the laboratory turbine is a geometrically-scaled model, then c/R and N are constant. Further, ρ and ρ_b are likely to be similar between scales and, in a Reynolds independent regime $\langle C_Q, c \rangle$ would be constant. Consequently, for a given tip-speed ratio,

$$\frac{t_i^f}{t_i^l} = \frac{U_o^l}{U_o^f} \frac{L^f}{L^l}. \tag{28}$$

Consequently, if experiments are conducted in a laboratory-scale facility with similar inflow velocity to a field setting, then t_i would be proportional to the geometric scale of the model and the laboratory turbine would be more responsive to equivalent frequencies of turbulence than the field

ACCEPTED MANUSCRIPT

AIP Publishing

This manuscript was accepted by Renewable Sustainable Energy. Click here to see the version of record.

turbine. While this suggests that matching t_i across scales could be achieved by reducing inflow velocity in the laboratory, this would make it more difficult to achieve Reynolds independence and would reduce the signal-to-noise ratio in force and torque measurements. A more effective approach would be to artificially increase the rotational moment of inertia in the laboratory by using a denser blade material, incorporating an auxiliary mass above the water surface, or emulating inertia by applying a time-varying control torque that opposes angular acceleration.

We note that there is an additional subtly to the above that depends on control scheme. When the turbine angular velocity is prescribed (e.g., speed-regulated control), scale has no effect on the blade kinematics and, therefore, on $\langle C_{Q,c} \rangle$. However, for control schemes where the turbine angular velocity is not prescribed, the variation in angular momentum during a rotation is equal to the difference between the hydrodynamic torque and control torque (Eq. 1). Because the blade kinematics (Eq. 16 and Eq. 17) depend on the non-dimensional rotational trajectory and the hydrodynamic torque coefficient depends on the blade kinematics (e.g., Fig. 8), the rotational hydrodynamics and kinematics are coupled under torque-regulated control for a cross-flow turbine. This gives rise to additional phase-average dynamics that may non-linearly affect $\langle C_{Q,c} \rangle$.

For axial-flow turbines, hydrodynamic torque is nearly invariant with azimuthal position, so torque-regulated control yields approximately constant rotational speed. Consequently, there is no significant distinction between control torque and hydrodynamic torque for any power take-off mechanism. Similarly, phase-average variations in hydrodynamic torque decrease for cross-flow turbines with increasing blade count or helix angle[25].

B. Use of Servomotors in Turbine Experiments

An intuitive objection to the use of a servomotor or a stepper motor as a power take-off mechanism in experiments is that electrical power can be supplied to it, which could artificially inflate the experimentally estimated $\langle C_{P,h} \rangle$. Because these motors can apply torque in the same direction as turbine rotation, they enable a wider range of operating conditions than purely resistive power take-off mechanisms and can maintain a constant rotational speed. As previously discussed, this does not increase $\langle C_{P,h} \rangle$. Indeed, for the turbine considered here, the maximum $\langle C_{P,h} \rangle$ is slightly higher under torque-regulated control than speed-regulated control as a consequence of differing blade kinematics. In experiments where the hydrodynamic torque is in the direction of rotation for all azimuthal positions (e.g., axial-flow turbines), these motors simply oppose rotation, much as a

ACCEPTED MANUSCRIPT

AIP Publishing

This manuscript was accepted by Renewable Sustainable Energy. Click here to see the version of record.

friction brake.

The use of servomotors in experiments has four primary benefits. First, as previously discussed, servomotors and stepper motors enable speed-regulated control, under which turbine dynamics are independent of the rotational moment of inertia. Second, for computational fluid dynamics of cross-flow turbines to be tractable, it is often necessary to impose a constant rotational speed[4]. Consequently, data from experiments utilizing servomotors are directly comparable to simulations. Third, servomotors allow more advanced control strategies to be employed, which can exploit hydrodynamics and kinematics to enhance turbine performance[10]. Fourth, servomotors allow starting and operating the turbine at relatively low inflow speeds, when hydrodynamic torque is insufficient to overcome static friction in the power take-off. Because the ratio of friction to hydrodynamic force is often larger in the laboratory than for full-scale systems, performance characterization in low-speed regimes is of commercial interest.

In field settings, generators coupled to control systems and energy sources can be configured for speed-regulated or torque-regulated control, as well as modes with phase variations in the control set point (e.g., intracycle control). Such motor/generator combinations are commonplace in the regenerative braking systems used in electrical vehicle power trains[26]. For current turbines, this choice of control schemes has implications for the strategy used to shed mechanical power above "rated" flow conditions. If regulation is by resistive torque and there is not an additional degree of freedom available (e.g., mechanically adjusting the blade pitch[27]), then the only way to shed power is by increasing the rotational speed and operating in an "overspeed" mode. However, this increases the structural loads on the turbine rotor (Fig. 6) and may increase the installed equipment cost. Under speed-regulated control, the turbine can shed power by decreasing rotational speed and operating in an "underspeed" mode.

Use of servomotors in laboratory experiments does present several challenges. First, the internal control logic on the motor drive and external feedback loop used in these experiments were tuned to produce nearly constant rotational speed or control torque. De-tuning this control logic can cause rotational speed and control torque to vary simultaneously, such that $\langle C_{P,h} \rangle$ departs from the performance that would be observed under truly constant control torque or rotational speed. Because experimental results are specific to the servomotor and drive tuning, phase-average performance should be reported to ensure that the intended control objectives are met. Second, servomotor drives can produce electromagnetic interference that increases electrical noise in torque and force measurements. Such interference can be mitigated by power and communication isolation

ACCEPTED MANUSCRIPT

AIP Publishing

This manuscript was accepted by Renewable Sustainable Energy. Click here to see the version of record.

between the servomotor drive and data acquisition hardware, as well as physically separating the drive from data acquisition hardware.

VI. CONCLUSIONS

Any control mode that results in net positive power for a cross-flow turbine may be of interest for energy harvesting, and all of these are net "fluid-driven". Speed-regulated control can be achieved using a servomotor or stepper motor, and this control mode allows turbine operation across all tip-speeds that produce net positive power. Torque-regulated control may be achieved using any electrical or mechanical power take-off, though the operating range is more limited when only a constant resistive control torque can be imposed. Differences in control strategies yield different blade kinematics which can affect time-average turbine performance. Consequently, the choice of control strategy is important and should be carefully considered in experimental design.

ACKNOWLEDGMENTS

The authors wish to acknowledge several helpful discussions with Dr. Martin Wosnik at the University of New Hampshire. The Alice C. Tyler Charitable Trust supported multiple upgrades to the experimental facilities at the University of Washington, including the higher flow speeds and closed-loop temperature control used in these experiments. Funding for this project was provided by the U.S. Department of Defense Naval Facilities Engineering Command. Hannah Ross is supported by the National Science Foundation Graduate Research Fellowship Program under Grant DGE-1256082.

Appendix A: Cycle-average Equivalence of Hydrodynamic and Control Power

The turbine equation of motion is

$$J\dot{\omega}(t) = Q_h(t) - Q_c(t). \tag{A1}$$

The instantaneous hydrodynamic power is

$$P_h(t) = \omega(t)Q_h(t), \tag{A2}$$

ACCEPTED MANUSCRIPT

AIP Publishing

This manuscript was accepted by Renewable Sustainable Energy. Click here to see the version of record.

and the average hydrodynamic power over a full rotation of duration T is

$$\langle P_h(t)\rangle = \frac{1}{T}\int_0^T \omega(t)Q_h(t)dt. \tag{A3}$$

Because we measure the control torque directly, rather than the hydrodynamic torque, the above must be reformulated in terms of Q_c. From the equation of motion,

$$Q_h(t) = J\dot{\omega}(t) + Q_c(t), \tag{A4}$$

so the hydrodynamic power can be expressed as

$$P_h(t) = J\omega(t)\dot{\omega}(t) + \omega(t)Q_c(t). \tag{A5}$$

The average hydrodynamic power is then

$$\langle P_h(t)\rangle = \frac{1}{T}\int_0^T [J\omega(t)\dot{\omega}(t) + \omega(t)Q_c(t)]dt = \frac{J}{T}\int_0^T \omega(t)\dot{\omega}(t)dt + \frac{1}{T}\int_0^T \omega(t)Q_c(t)dt. \tag{A6}$$

Let us consider the first integral on the right hand side. This term is the mean power associated with accelerating and decelerating the turbine, or

$$\langle P_{\text{acc}}(t)\rangle = \frac{J}{T}\int_0^T \omega(t)\dot{\omega}(t)dt. \tag{A7}$$

Using the definition of the angular acceleration,

$$\dot{\omega}(t) = \frac{d\omega(t)}{dt}, \tag{A8}$$

rearranging to

$$dt = \frac{d\omega(t)}{\dot{\omega}(t)}, \tag{A9}$$

and substituting into Eq. A7 with the corresponding change in integration limits yields

$$\langle P_{\text{acc}}(t)\rangle = \frac{J}{T}\int_{\omega(t=0)}^{\omega(t=T)} \omega(t)d\omega(t). \tag{A10}$$

Evaluating the integral yields

$$\langle P_{\text{acc}}(t)\rangle = \frac{J}{2T}\left[\omega(t=T)^2 - \omega(t=0)^2\right]. \tag{A11}$$

ACCEPTED MANUSCRIPT

AIP Publishing

This manuscript was accepted by Renewable Sustainable Energy. Click here to see the version of record.

If the turbine velocity is periodic, $\omega(t=T)=\omega(t=0)$. Thus,

$$\langle P_{\text{acc}}(t)\rangle = 0. \tag{A12}$$

Therefore, the mean hydrodynamic power given in Eq. A6 becomes

$$\langle P_h(t)\rangle = \frac{1}{T}\int_0^T \omega(t)Q_c(t)dt \tag{A13}$$

Consequently, as long as periodicity is enforced and the average is taken over an integer number of turbine rotations, n, the mean hydrodynamic power can be calculated by using the measured control torque rather than the hydrodynamic torque, or

$$\langle P_h(t)\rangle = \frac{1}{nT}\int_0^{nT} \omega(t)Q_h(t)dt = \frac{1}{nT}\int_0^{nT} \omega(t)Q_c(t)dt. \tag{A14}$$

A similar derivation appears in Strom et al.[10].

We compare this theoretical result to experimental performance in Fig. 10, calculating hydrodynamic torque from measurements (Eq. A4). Under speed-regulated control, $\langle \omega Q_h\rangle \approx \langle \omega Q_c\rangle$ over most of the performance curve, with only slight deviations at the highest tip-speed ratios. This is likely a consequence of the difficulty of maintaining servomotor speed under a relatively high thrust load. However, under torque-regulated control the deviation between $\langle \omega Q_h\rangle$ and $\langle \omega Q_c\rangle$ is observable over a range of tip speeds and becomes experimentally significant at high tip speeds. This is because under torque-regulated control, turbine velocity is not guaranteed to be periodic, such that Eq. A12 is no longer satisfied. Further, at high tip-speed ratios, the signal-to-noise ratio for closed-loop torque control is degraded. Consequently, if the experimental objective is to characterize the hydrodynamic performance of a turbine, characteristic performance should be presented in terms of $\langle C_{P,h}\rangle$. For both control schemes, the variation between $\langle \omega Q_h\rangle$ and $\langle \omega Q_c\rangle$ is accounted for by a net accumulation or loss of rotational kinetic power in the turbine assembly.

Appendix B: Turbine Geometry Definitions

We define the turbine radius, R, as the distance from the axis of rotation to the outer surface of the foil at the quarter-chord. The turbine height is defined as the distance between the outer faces of the blade mounting structures (i.e., foil-shaped struts). These definitions mean that the projected

ACCEPTED MANUSCRIPT

AIP Publishing

This manuscript was accepted by Renewable Sustainable Energy. Click here to see the version of record.

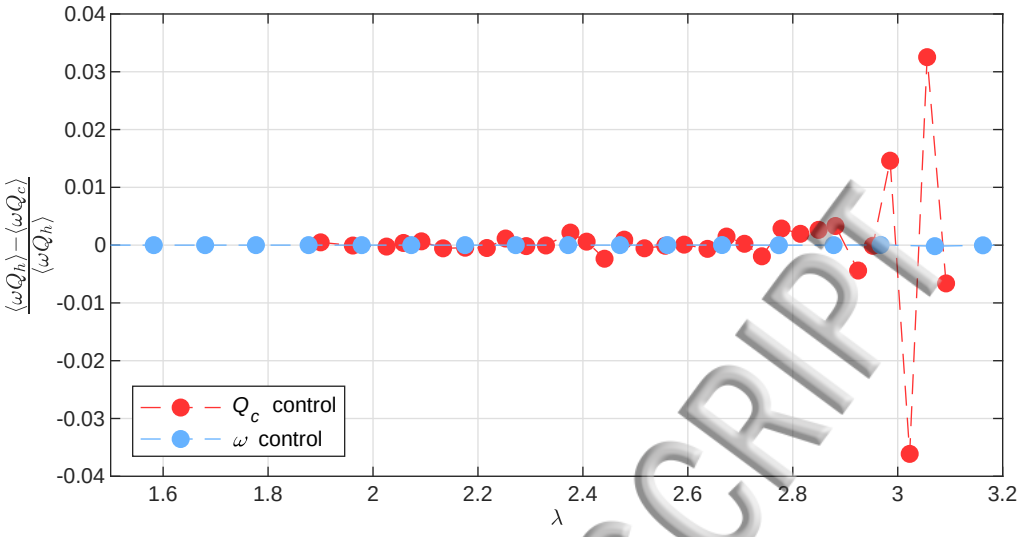


FIG. 10. Comparison of time-average hydrodynamic and control power under speed-regulated and torque-regulated control.

area, A, used to normalize torque, power, and force coefficients corresponds to a rectangle enclosing the turbine rotor. The projected area of shaft couplings and drive shaft outside of this rectangle are not included in A as they negligibly affect hydrodynamic torque. These are, however, $\sim 8\%$ of A and meaningfully affect thrust. Consequently, if this experiment were to be repeated with a drive shaft of different dimensions, but all other parameters held constant, the thrust coefficient would change. Adopting a different definition of A for the thrust coefficient would address this inconsistency, but would likely cause more confusion than is warranted.

The definition of turbine radius also leads to an inconsistency in calculating the nominal angle of attack (Eq. 16). The relative inflow velocity is the vector sum of the velocity in the direction normal to and tangential to blade motion. The entire blade is assumed to have a tangential speed of ωR, but this is only true for points on the blade surface that are actually at distance R from the axis of rotation. For turbines where c/R is "small", this approximation is of little consequence, but when this is not the case, each point on the blade surface has a different tangential speed. This produces an azimuthal variation in virtual camber[28] and also complicates interpretation of the angle of attack at the leading edge of the foil. This inconsistency is, however, likely insignificant in comparison to neglecting the effects of induction on normal and tangential velocity.

ACCEPTED MANUSCRIPT

AIP Publishing

This manuscript was accepted by Renewable Sustainable Energy. Click here to see the version of record.

Appendix C: Inflow Velocity Time Correction

The time correction (i.e., lag), t_l, between when inflow velocity is sampled by the ADV and when it interacts with the rotor can be estimated from Taylor's hypothesis as

$$t_l = \frac{L}{\langle U_o \rangle} \tag{C1}$$

where L is the distance between the ADV and turbine (here, $5D$). At a nominal inflow velocity of 1 m/s, this implies $t_l = 0.9$ s. However, inflow velocity was recorded by the manufacturer's software, which has a time stamp bias of up to 1 s and, in addition, streamwise induction dilates t_l. Therefore, an empirical estimate of t_l was derived from the cross-correlation between low-pass filtered inflow velocity and hydrodynamic turbine power, P_h. This exploits the time scale separation between the dominant turbulent excitation frequency in the flume and the dominant intracycle periodicity in hydrodynamic power (Appendix E). For speed-regulated control, a 5 s moving-average filter yielded $t_l = 2.1 \pm 0.2$ s with peak correlation coefficients > 0.9 in the region of interest for power generation. A representative example is shown in Fig. 11. Under torque-regulated control, this method yielded similar lag times, but with lower correlation coefficients. Consequently, $t_l = 2.1$ s was taken as an estimate for all control set points under torque-regulated and speed-regulated control.

Appendix D: Experimental Repeatability

These experiments were conducted three times, holding all variables constant except, during the first trial, an open-loop torque command was sent from the DAQ to the motor drive. For all three trials, the turbine was marched through set points under speed-regulated control and torque-regulated control without being removed from the flume. Between trials, the turbine, upper assembly constraining the servo motor and load cell, and suction plate containing the bearing and lower load cell were removed and reinstalled. Chronologically, the second trial is the "production" case used in the body of this paper and the third trial was used to verify consistency. As shown in Fig. 12, moderately better repeatability was achieved under speed-regulated control than torque-regulated control. However, the overall deviation in performance between the trials was similar under both control schemes and the time-average performance overlapped within the interquartile range for cycle-average performance.

ACCEPTED MANUSCRIPT

AIP Publishing

This manuscript was accepted by Renewable Sustainable Energy. Click here to see the version of record.

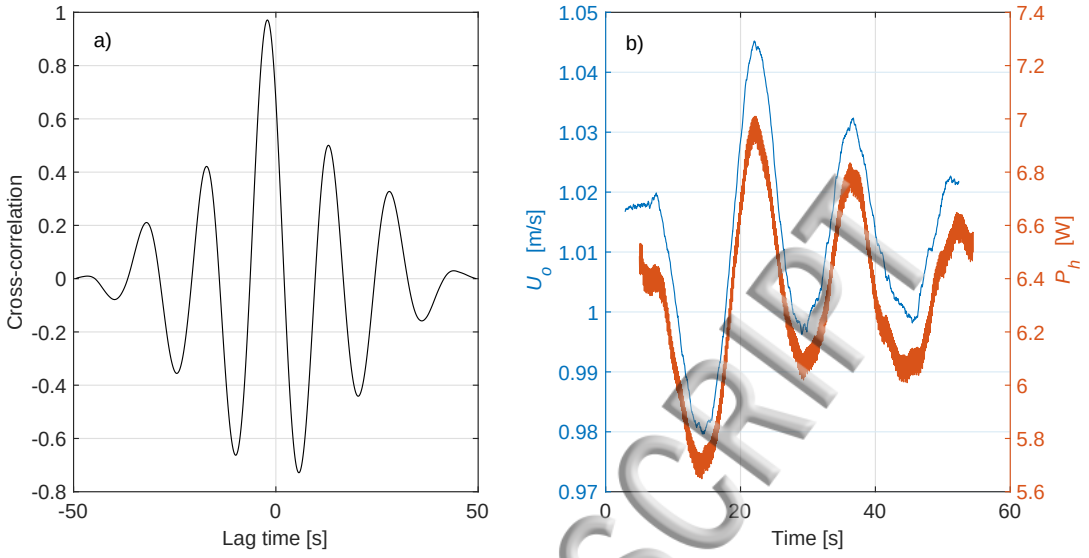


FIG. 11. Representative results from time lag evaluation. (a) Cross-correlation at each time lag. The correlation peak occurs at -2.1 s. (b) Hydrodynamic power and time-lagged inflow velocity with 5 s moving-average filter applied.

Appendix E: Effect of Turbulence

The interplay between turbulence and turbine inertia is well-established for axial-flow turbines, where, for example, frequency-domain fluctuations in turbine power can be described by a transfer function acting on frequency-domain fluctuations in the inflow fluid speed[6,29]. As shown in Fig. 13, the dominant periodicity in power, thrust, and lateral force for a two-bladed cross-flow turbine is twice-per-rotation (Fig. 13b-d), with a secondary periodicity once-per-rotation associated with minor asymmetry. While turbulence intensity is 2 %, this is primarily a low-frequency oscillation (Fig. 13a, 14 s period), likely attributable to a resonance between the pumps and flume structure. This periodicity is apparent in turbine performance, but is at least two orders of magnitude less energetic than the intracycle periodicity. As a consequence, the energy-containing turbulence interacts with the turbine as an "engulfing gust" and the inflow velocity over a single rotation is approximately constant.

This leads to some observations about the cycle-to-cycle variations in $C_{P,h}$ and λ. These are shown in Fig. 14 under speed-regulated and torque-regulated control near the peak of the performance curves (corresponding to the control set points highlighted in Fig. 6). The variations in cycle-average $C_{P,h}$ and λ are similar under both strategies, but there is more variability in both

ACCEPTED MANUSCRIPT

AIP Publishing

This manuscript was accepted by Renewable Sustainable Energy. Click here to see the version of record.

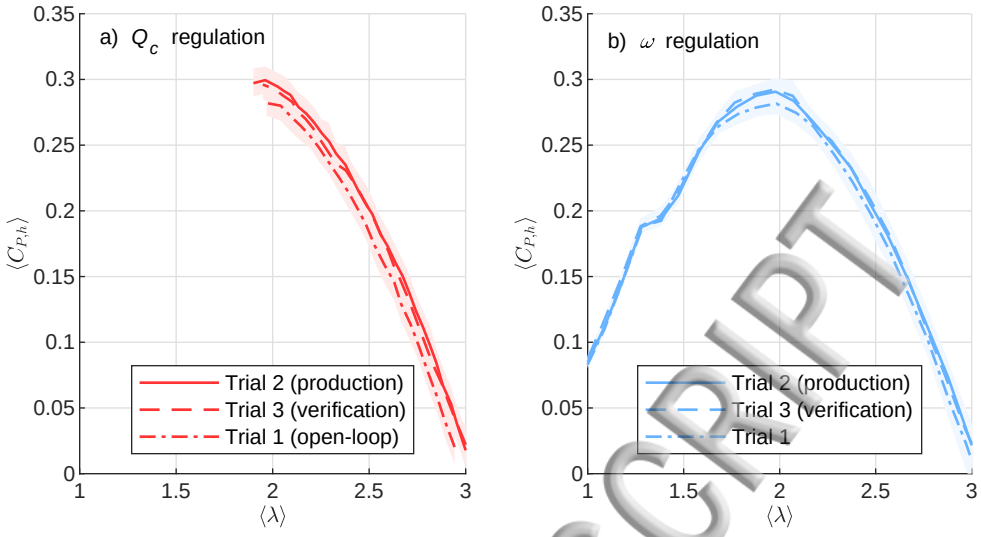


FIG. 12. Comparison of time-average characteristic performance across experimental trials under a) torque-regulated control and b) speed-regulated control.

quantities under torque-regulated control. This is because ω can fluctuate in response to changes in Q_h that arise from variations in U_o. As discussed in Tobin et al.[6], the interplay between turbulence and rotational inertia leads to an impulse-responses behavior under torque-regulated control that is absent under speed-regulated control.

However, the cycle-to-cycle variation observed in $\langle C_{P,h} \rangle$ under speed-regulated control is somewhat contradictory. On one hand, given that variations in $\langle \lambda \rangle$ depend on U_o, while those in $\langle C_{P,h} \rangle$ depend on U_o^3, one might anticipate a wider range of $\langle C_{P,h} \rangle$ than in $\langle \lambda \rangle$, as is apparent in Fig. 14b. However, the source of variation in $\langle C_{P,h} \rangle$ at a given $\langle \lambda \rangle$ is less intuitive. This may simply be the limit of experimental uncertainty, with scatter from measurement noise and temporal mismatch between turbine power and inflow velocity; the latter arising from the approximate inflow time correction (Appendix C). However, this could also arise from cycle-to-cycle differences in dynamic stall, which could be explored through time-resolved flow-field visualization inside the turbine rotor.

Finally, we note that under torque-regulated control, there is a slight deviation between the median of cycle-average performance and the time-average (Fig. 14). This is a consequence of the variations in cycle duration under this control scheme, which means that the time-average performance is biased towards cycles with lower average rotational speeds. Because time-average performance is of primary interest, in Fig. 5 and Fig. 6 the interquartile range in cycle-average

ACCEPTED MANUSCRIPT

AIP Publishing

This manuscript was accepted by Renewable Sustainable Energy. Click here to see the version of record.

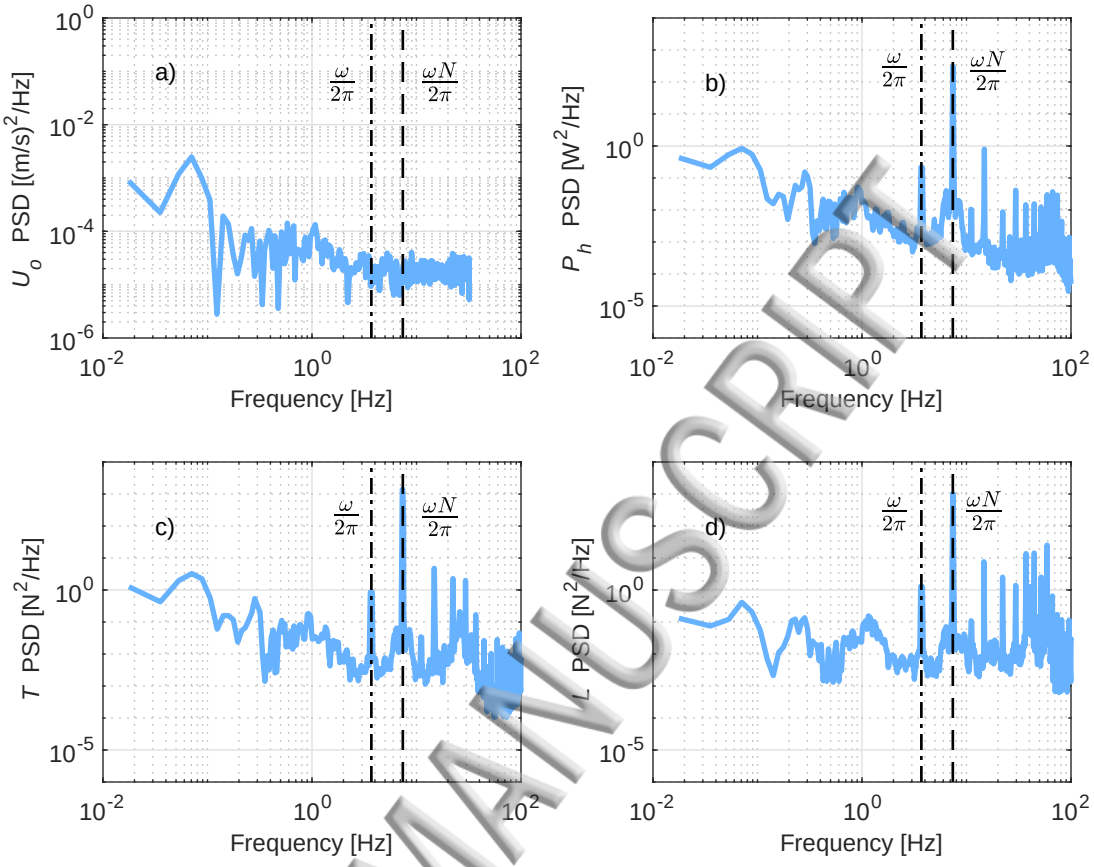


FIG. 13. Power spectral density at maximum $\langle C_{P,h} \rangle$ under speed-regulated control for (a) inflow velocity, (b) hydrodynamic power, (c) thrust, and (d) lateral force. The dash-dot line denotes the turbine rotation rate ($\frac{\omega}{2\pi}$) and the dashed line denotes the fundamental blade passing frequency ($\frac{\omega N}{2\pi}$).

performance is centered on the time-average, rather than cycle-average median.

REFERENCES

[1]R. Howell, N. Qin, J. Edwards, and N. Durrani, "Wind tunnel and numerical study of a small vertical axis wind turbine," Renewable energy **35**, 412–422 (2010).

[2]L. A. Danao, O. Eboibi, and R. Howell, "An experimental investigation into the influence of unsteady wind on the performance of a vertical axis wind turbine," Applied Energy **107**, 403–411 (2013).

[3]D. B. Araya and J. O. Dabiri, "A comparison of wake measurements in motor-driven and flow-

ACCEPTED MANUSCRIPT

AIP Publishing

This manuscript was accepted by Renewable Sustainable Energy. Click here to see the version of record.

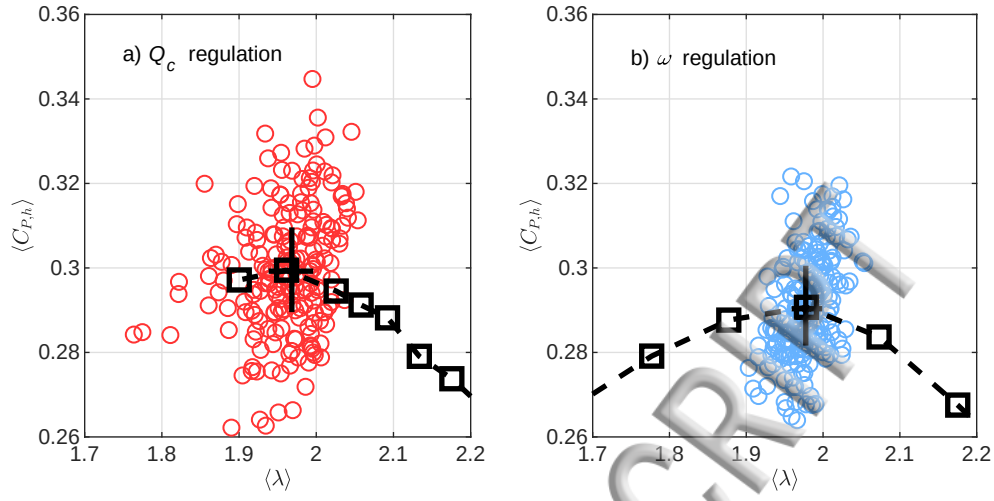


FIG. 14. Comparison of cycle-average performance variation under a) torque-regulated control and b) speed-regulated control. Open black squares denote time-average $\langle C_{P,h} \rangle$ and $\langle \lambda \rangle$ for control set points. Colored circles denote average performance over a single cycle at the set point corresponding to the maximum power coefficient under torque-regulated control and the closest equivalent set point under speed-regulated control. Solid black lines denote the inter-quartile range for cycle-average performance, centered on the median performance for all cycles at this control set point.

driven turbine experiments," Experiments in Fluids **56**, 150 (2015).

[4]A. Buchner, M. Lohry, L. Martinelli, J. Soria, and A. Smits, "Dynamic stall in vertical axis wind turbines: comparing experiments and computations," Journal of Wind Engineering and Industrial Aerodynamics **146**, 163–171 (2015).

[5]M. A. Miller, S. Duvvuri, I. Brownstein, M. Lee, J. O. Dabiri, and M. Hultmark, "Vertical-axis wind turbine experiments at full dynamic similarity," Journal of Fluid Mechanics **844**, 707–720 (2018).

[6]N. Tobin, H. Zhu, and L. Chamorro, "Spectral behaviour of the turbulence-driven power fluctuations of wind turbines," Journal of Turbulence **16**, 832–846 (2015).

[7]N. Fujisawa and S. Shibuya, "Observations of dynamic stall on darrieus wind turbine blades," Journal of Wind Engineering and Industrial Aerodynamics **89**, 201–214 (2001).

[8]L. Chamorro, C. Hill, S. Morton, C. Ellis, R. Arndt, and F. Sotiropoulos, "On the interaction between a turbulent open channel flow and an axial-flow turbine," Journal of Fluid Mechanics **716**, 658–670 (2013).

[9]P. Bachant and M. Wosnik, "Performance measurements of cylindrical-and spherical-helical

ACCEPTED MANUSCRIPT

AIP Publishing

This manuscript was accepted by Renewable Sustainable Energy. Click here to see the version of record.

cross-flow marine hydrokinetic turbines, with estimates of exergy efficiency," Renewable Energy **74**, 318–325 (2015).

[10]B. Strom, S. L. Brunton, and B. Polagye, "Intracycle angular velocity control of cross-flow turbines," Nature Energy **2**, 17103 (2017).

[11]I. Paraschivoiu, *Wind turbine design: with emphasis on Darrieus concept* (Presses inter Polytechnique, 2002).

[12]Y. Dai and W. Lam, "Numerical study of straight-bladed darrieus-type tidal turbine," Proceedings of the Institution of Civil Engineers-Energy **162**, 67–76 (2009).

[13]K. J. Ryan, F. Coletti, C. J. Elkins, J. O. Dabiri, and J. K. Eaton, "Three-dimensional flow field around and downstream of a subscale model rotating vertical axis wind turbine," Experiments in Fluids **57**, 38 (2016).

[14]M. Somoano and F. Huera-Huarte, "Flow dynamics inside the rotor of a three straight bladed cross-flow turbine," Applied Ocean Research **69**, 138–147 (2017).

[15]D. G. Goring and V. I. Nikora, "Despiking acoustic doppler velocimeter data," Journal of Hydraulic Engineering **128**, 117–126 (2002).

[16]B. Strom, N. Johnson, and B. Polagye, "Impact of blade mounting structures on cross-flow turbine performance," Journal of Renewable and Sustainable Energy **10**, x–x (2018).

[17]P. Bachant and M. Wosnik, "Effects of reynolds number on the energy conversion and near-wake dynamics of a high solidity vertical-axis cross-flow turbine," Energies **9**, 73 (2016).

[18]R. Cavagnaro and B. Polagye, "Stall dynamics of a cross-flow turbine," in *Marine Energy Technology Symposium* (2016).

[19]D. B. Araya, T. Colonius, and J. O. Dabiri, "Transition to bluff-body dynamics in the wake of vertical-axis wind turbines," Journal of Fluid Mechanics **813**, 346–381 (2017).

[20]E. N. Jacobs and A. Sherman, "Airfoil section characteristics as affected by variations of the reynolds number," Tech. Rep. NACA-TR-586 (National Advisory Committee for Aeronautics, 1937).

[21]G. J. Leishman, *Principles of helicopter aerodynamics with CD extra* (Cambridge university press, 2006).

[22]G. A. Van Kuik, "The lanchester–betz–joukowsky limit," Wind Energy: An International Journal for Progress and Applications in Wind Power Conversion Technology **10**, 289–291 (2007).

[23]D. Vandenberghe, D. Vandenburghe, and E. Dick, "Optimum pitch control for vertical axis wind turbines," Wind Engineering , 237–247 (1987).

ACCEPTED MANUSCRIPT

AIP Publishing

This manuscript was accepted by Renewable Sustainable Energy. Click here to see the version of record.

[24]I. Paraschivoiu, O. Trifu, and F. Saeed, "H-darrieus wind turbine with blade pitch control," International Journal of Rotating Machinery **2009** (2009).

[25]D. Forbush, R. Cavagnaro, and B. Polagye, "Power-tracking control for cross-flow wurbines," Journal of Renewable and Sustainable Energy **X** (in review).

[26]S. Cikanek and K. Bailey, "Regenerative braking system for a hybrid electric vehicle," in *American Control Conference, 2002. Proceedings of the 2002*, Vol. 4 (IEEE, 2002) pp. 3129–3134.

[27]B. Kirke and L. Lazauskas, "Limitations of fixed pitch darrieus hydrokinetic turbines and the challenge of variable pitch," Renewable Energy **36**, 893–897 (2011).

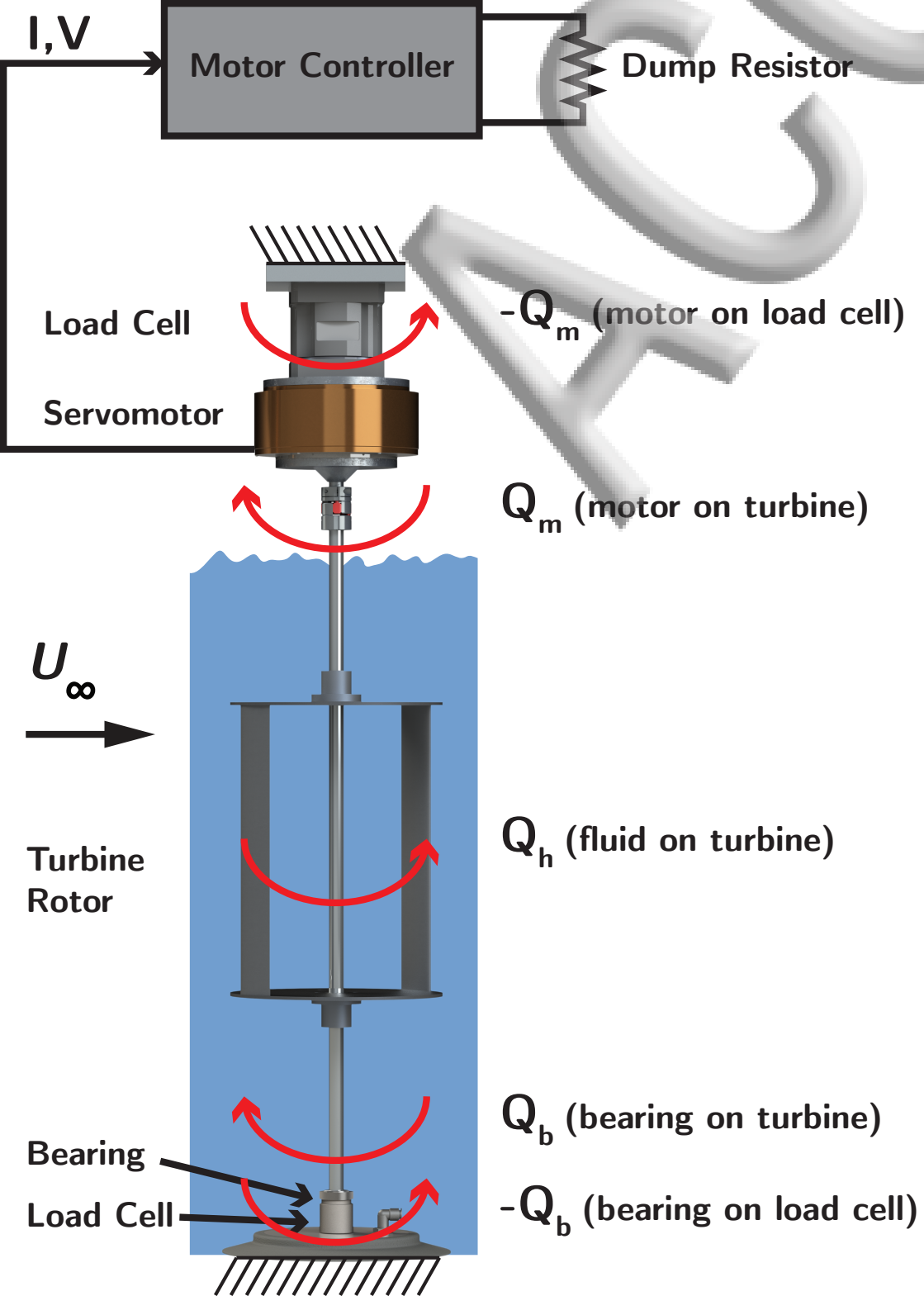
[28]P. G. Migliore, W. P. Wolfe, and J. B. Fanucci, "Flow curvature effects on darrieus turbine blade aerodynamics," Journal of Energy **4**, 49–55 (1980).

[29]Y. Jin, S. Ji, and L. P. Chamorro, "Spectral energy cascade of body rotations and oscillations under turbulence," Physical Review E **94**, 063105 (2016).

[30]L. Y. Pao and K. E. Johnson, "Control of wind turbines," IEEE Control Systems **31**, 44–62 (2011).

[31]D. Forbush, R. J. Cavagnaro, J. Donegan, J. McEntee, and B. Polagye, "Multi-mode evaluation of power-maximizing cross-flow turbine controllers," International journal of marine energy **20**, 80–96 (2017).

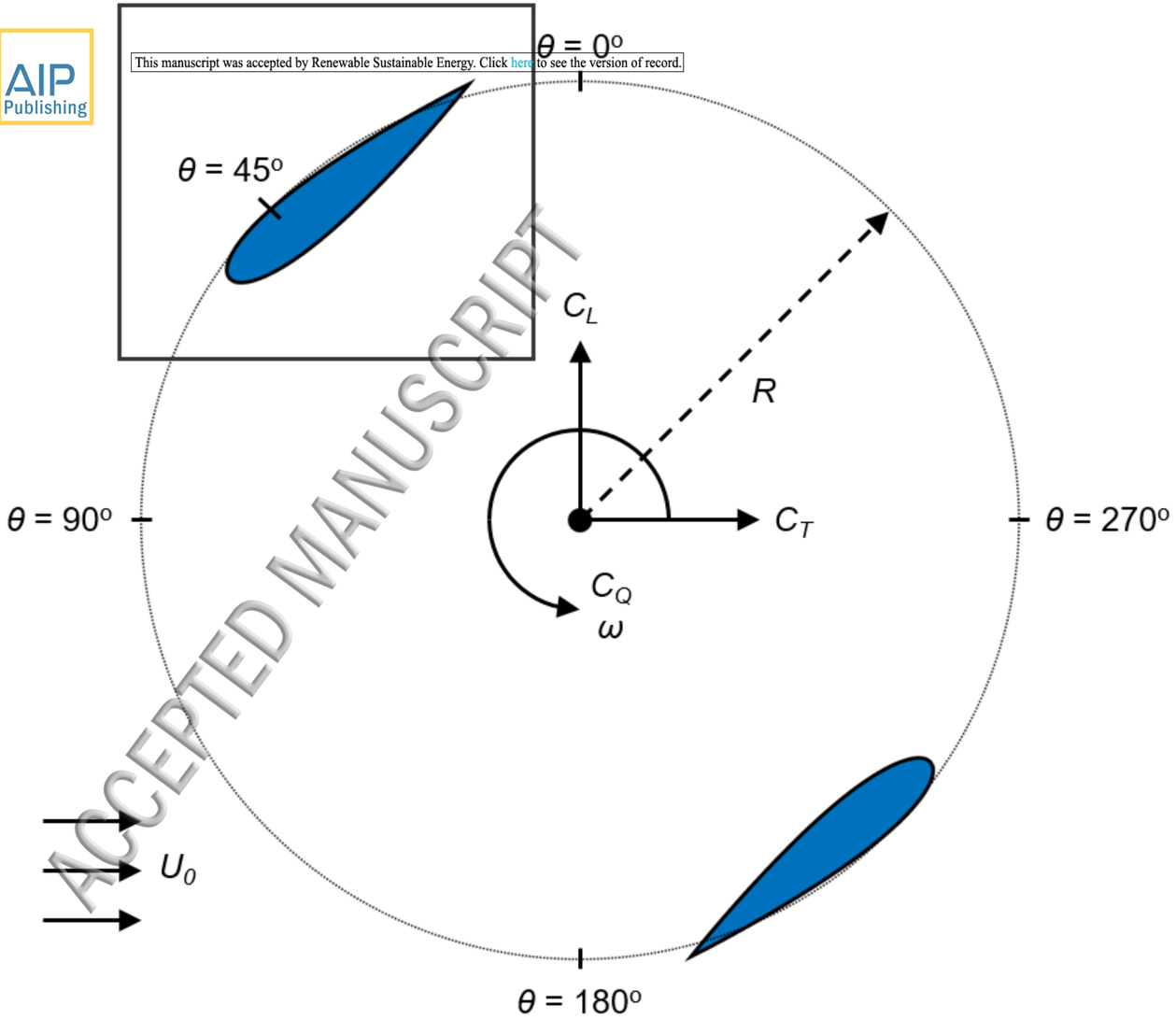
ACCEPTED MANUSCRIPT

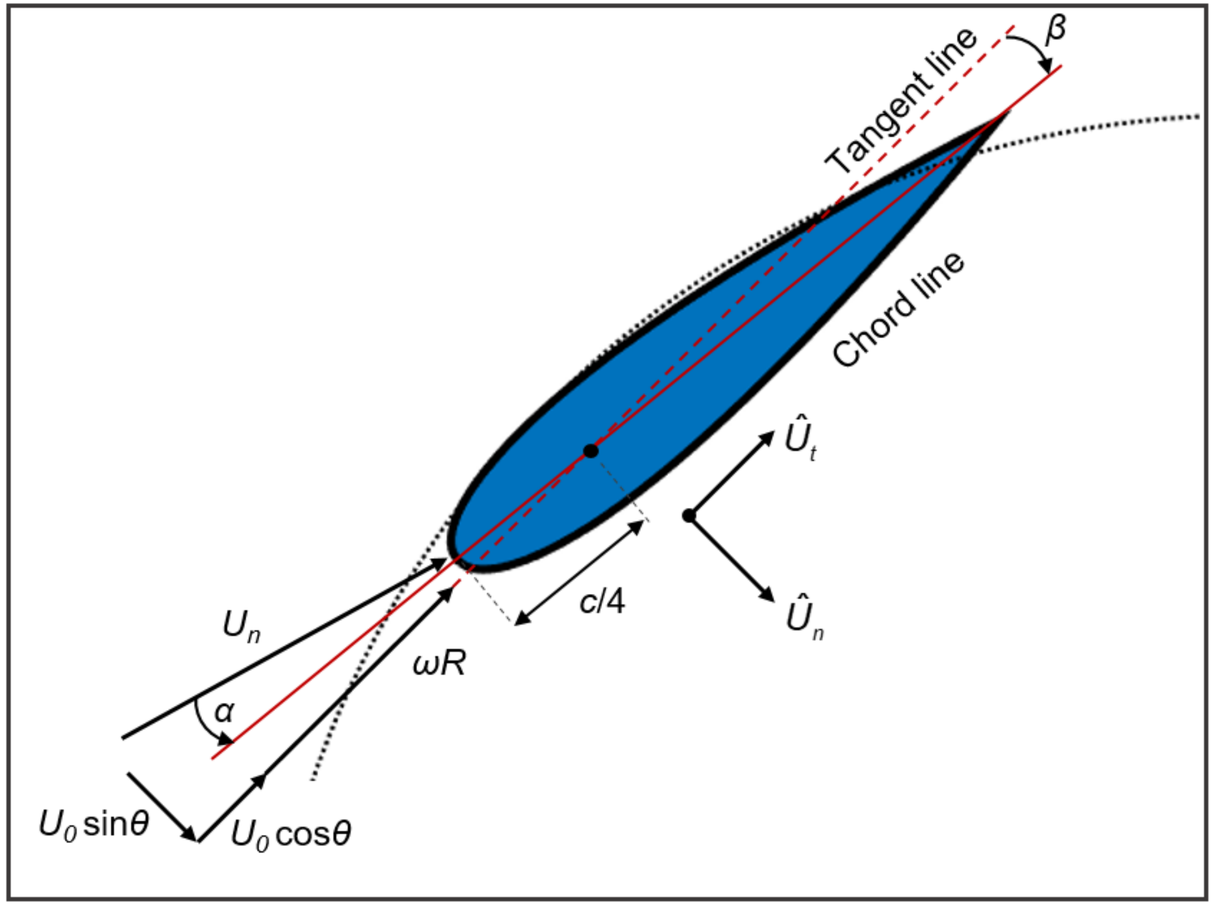

I,V
Motor Controller
Dump Resistor
Load Cell
Servomotor
$-Q_m$ (motor on load cell)
Q_m (motor on turbine)
U_∞
Turbine
Rotor
Q_h (fluid on turbine)
Q_b (bearing on turbine)
Bearing
Load Cell
$-Q_b$ (bearing on load cell)

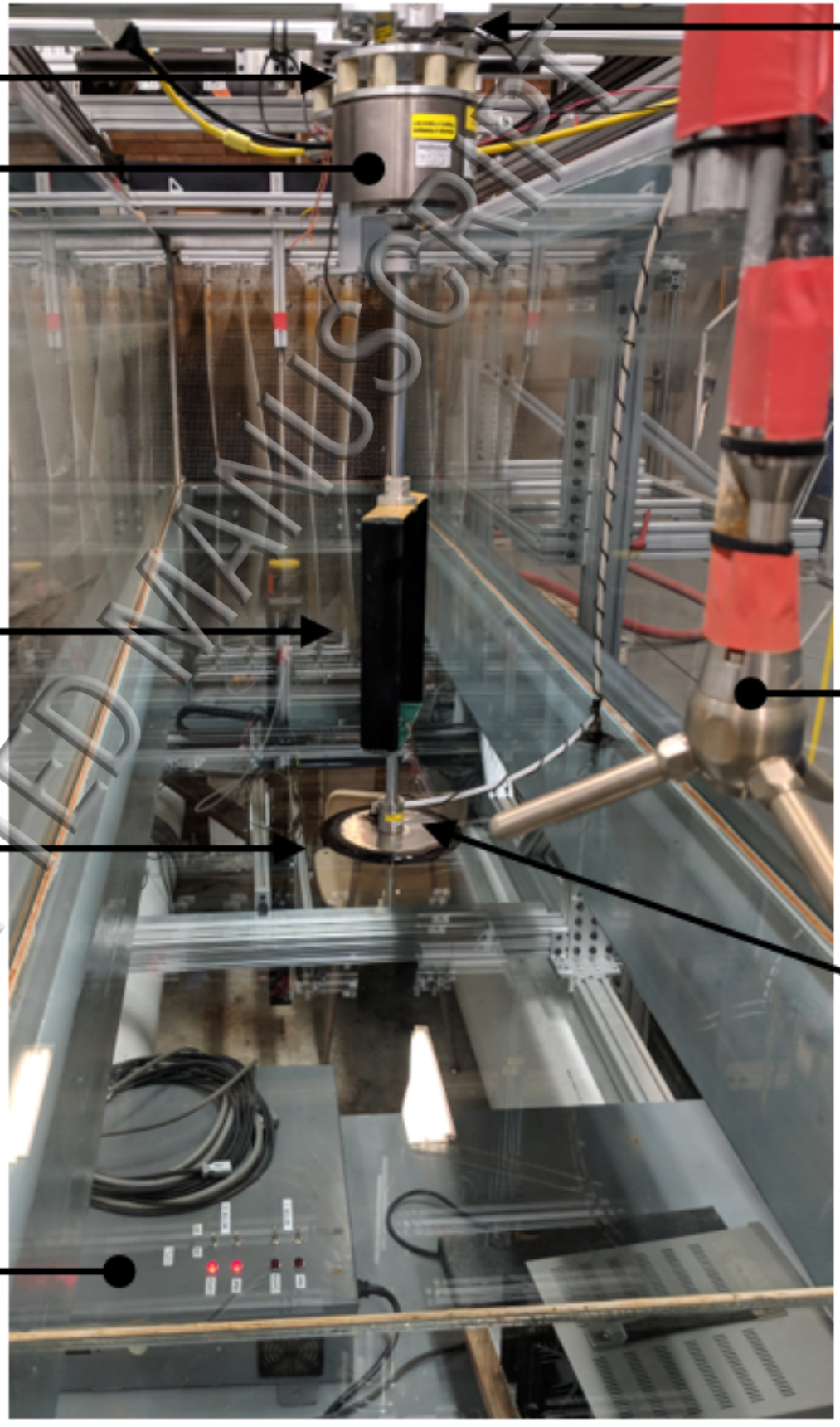
AIP Publishing

This manuscript was accepted by Renewable Sustainable Energy. Click here to see the version of record.

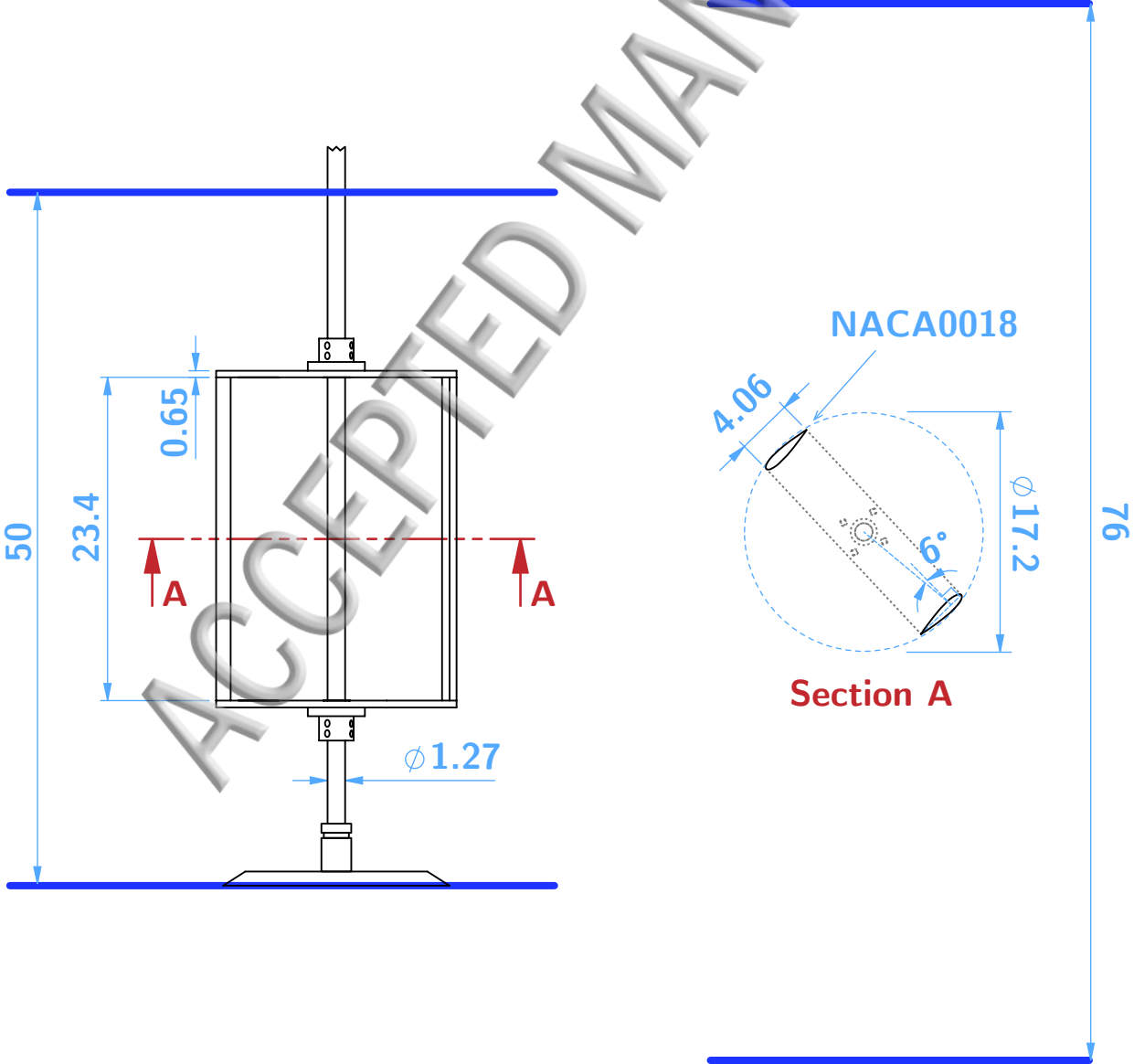
ACCEPTED MANUSCRIPT







ACCEPTED MANUSCRIPT

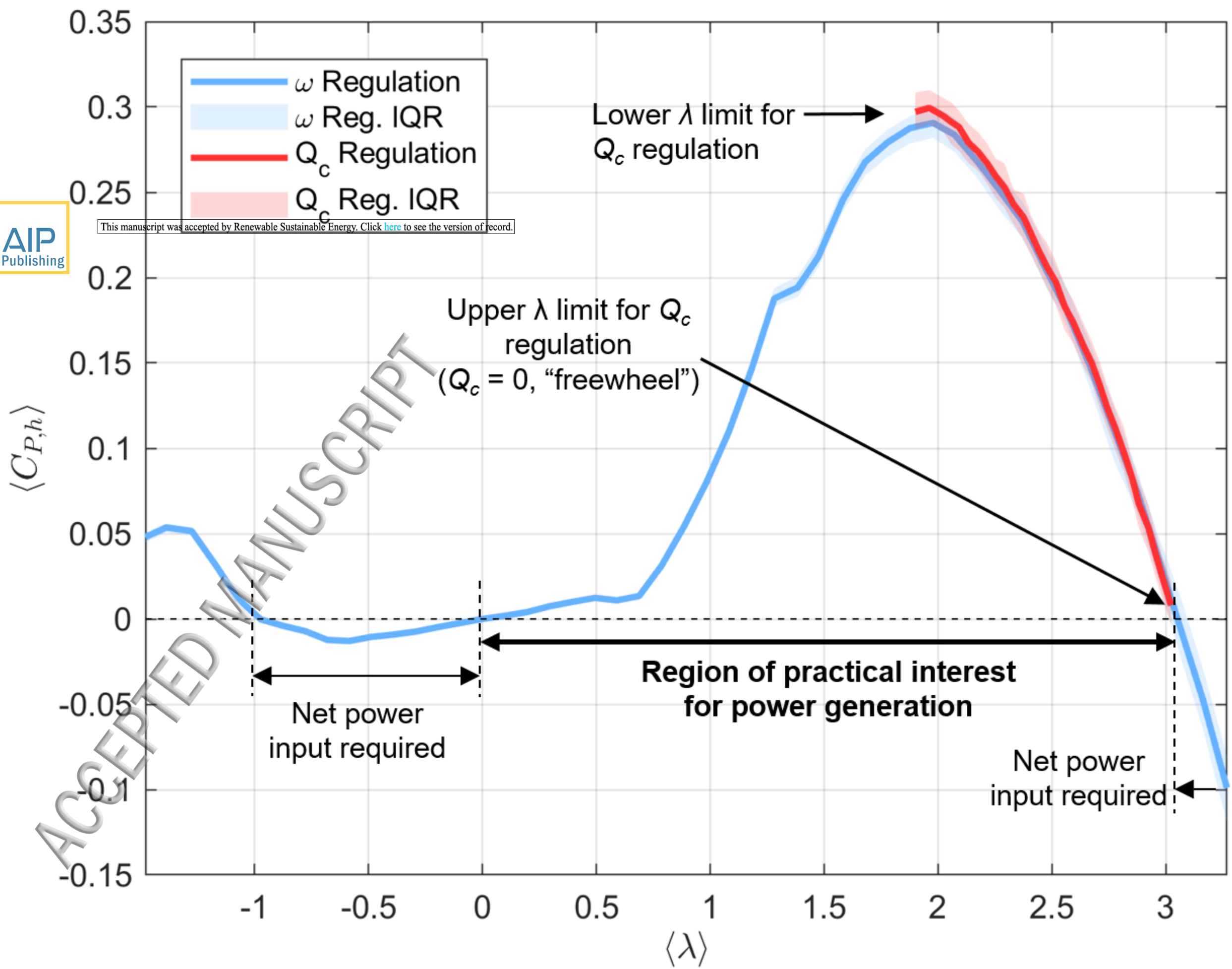


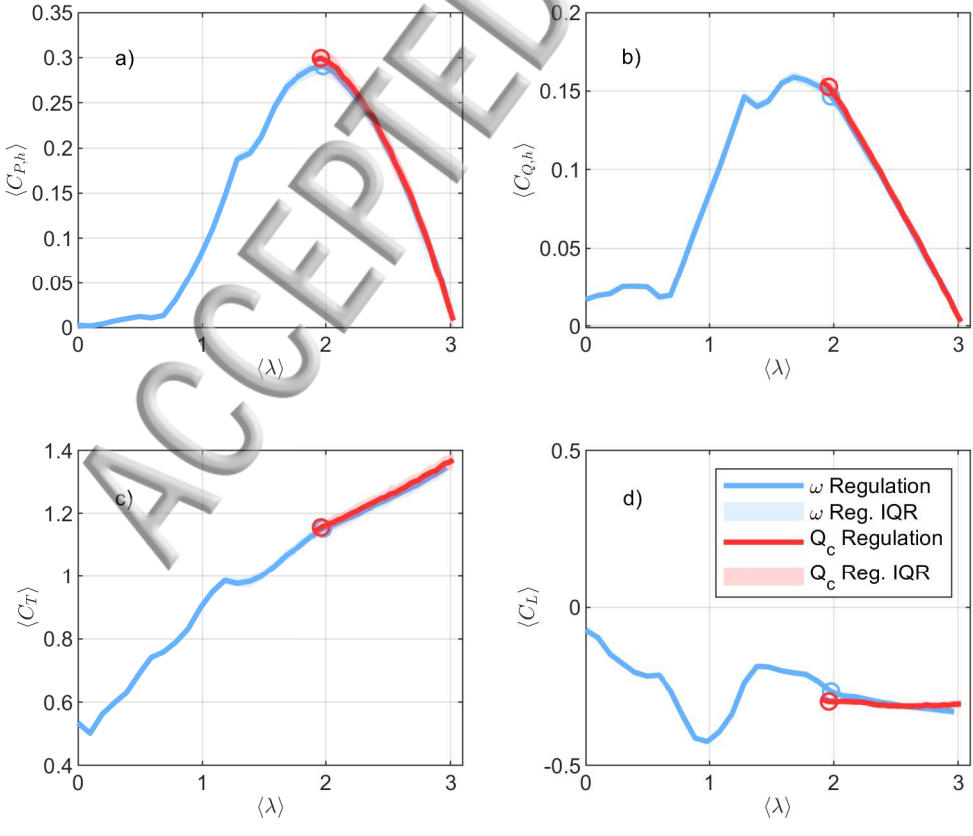
ACCEPTED MANUSCRIPT

AIP Publishing

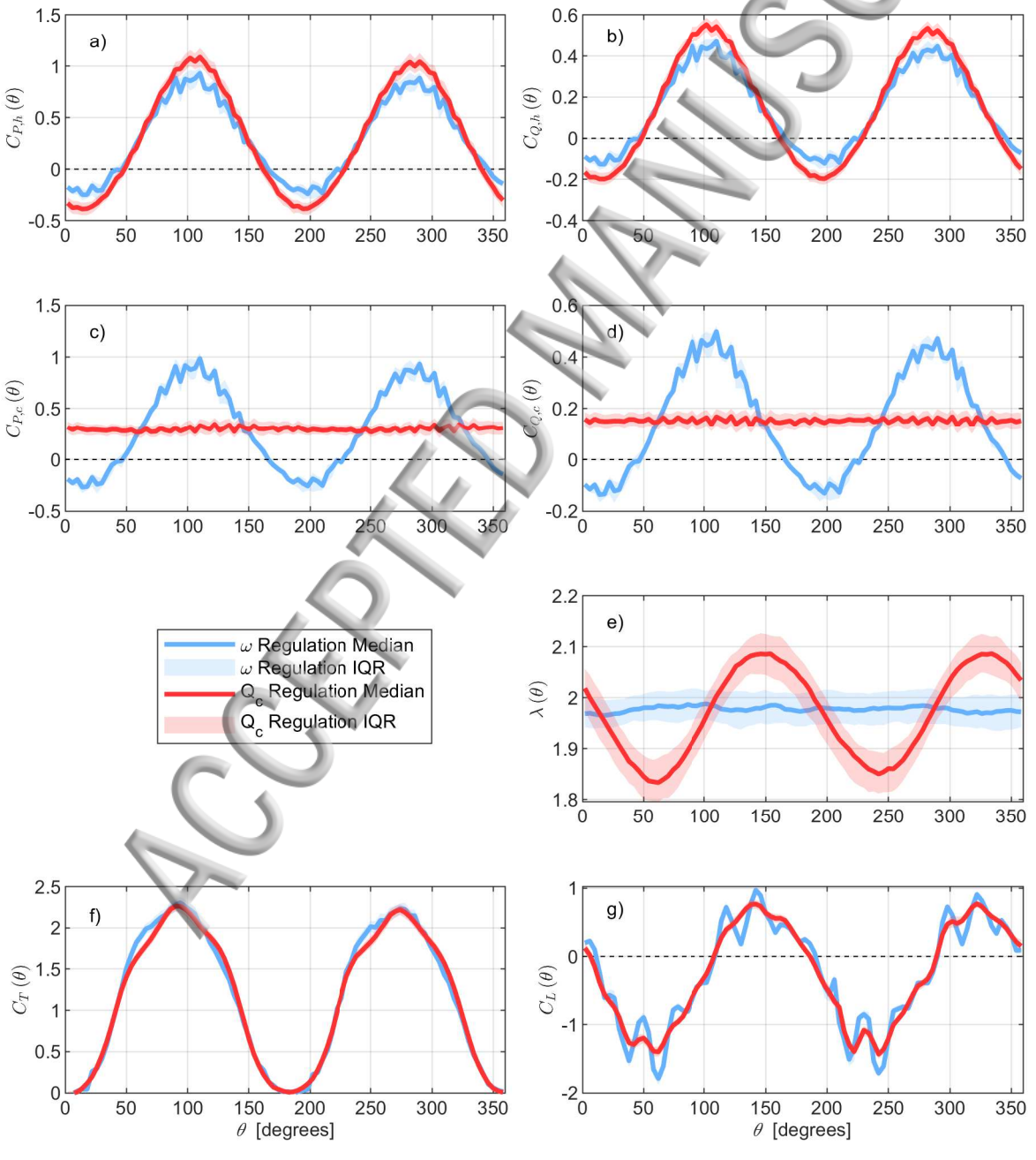
This manuscript was accepted by Renewable Sustainable Energy. Click here to see the version of record.

ACCEPTED MANUSCRIPT

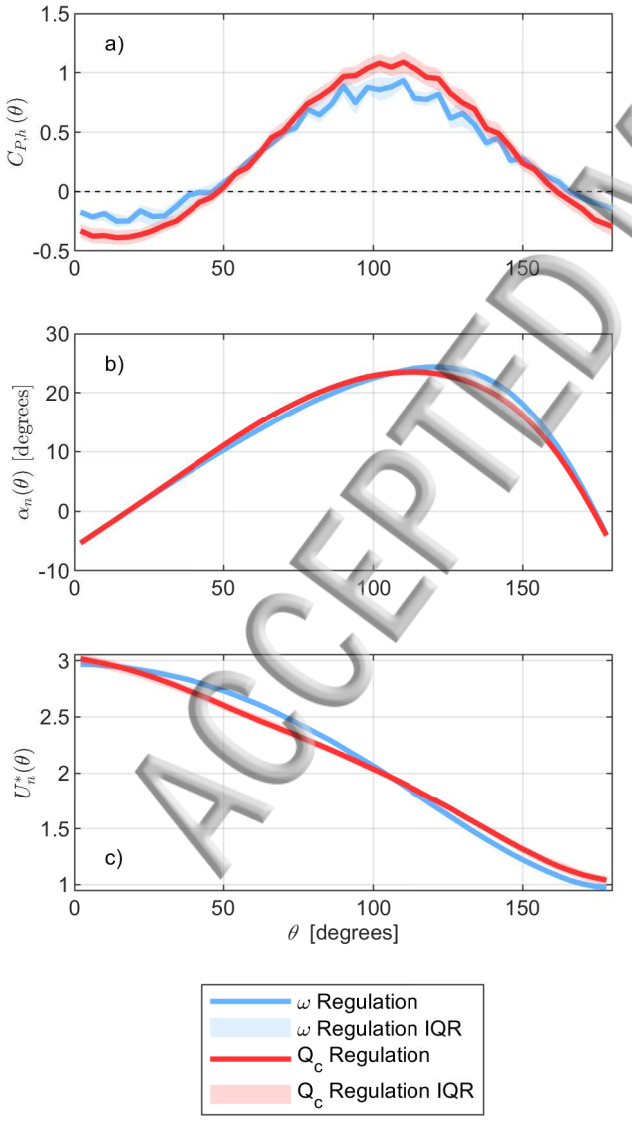



a)
b)
c)
d)
$\langle C_{P,h} \rangle$
$\langle C_{Q,h} \rangle$
$\langle C_T \rangle$
$\langle C_L \rangle$
$\langle \lambda \rangle$
ω Regulation
ω Reg. IQR
Q_c Regulation
Q_c Reg. IQR

ACCEPTED



ACCEPTED MANUSCRIPT

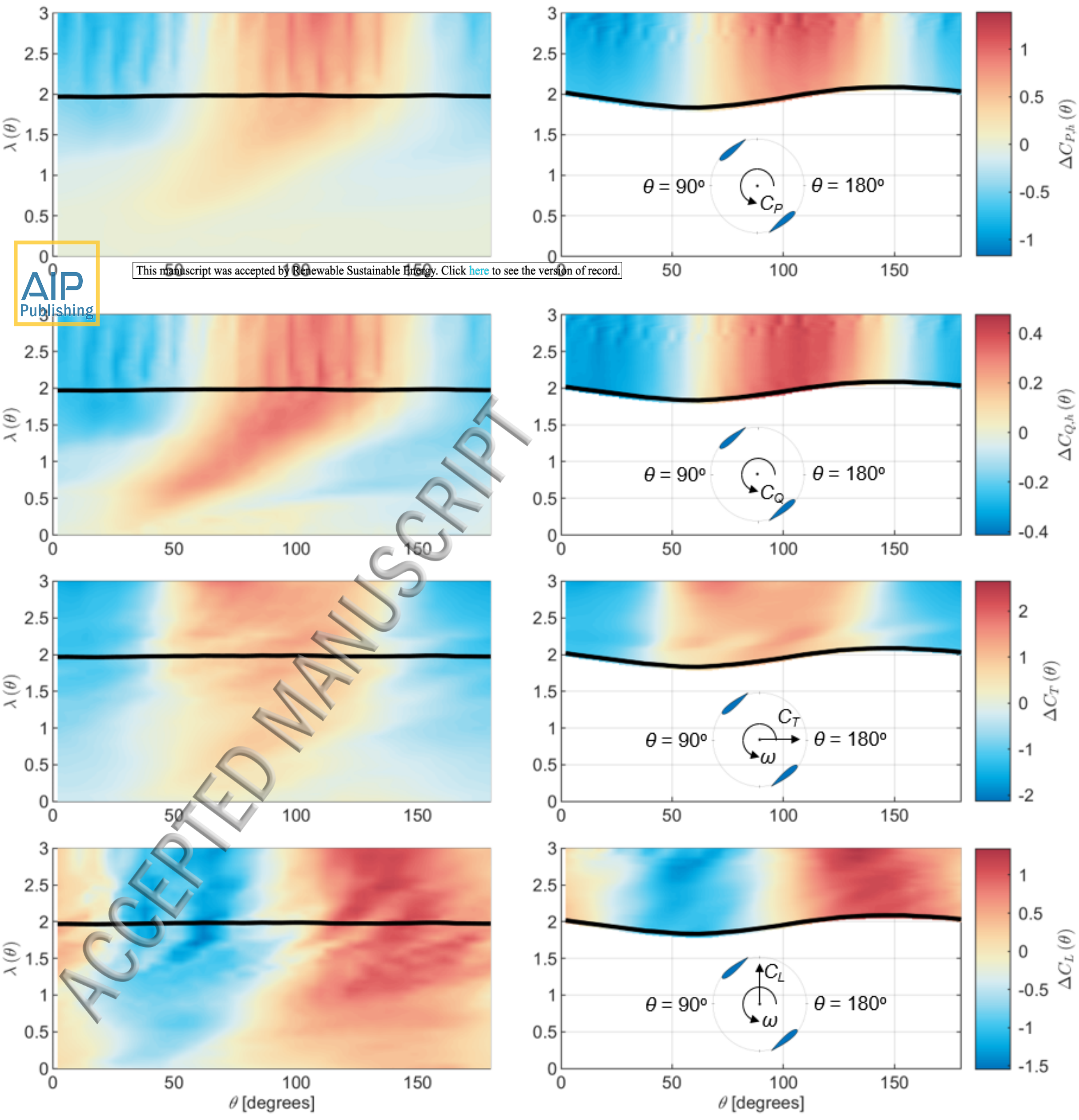

a)
$C_{P,h}(\theta)$
1.5
1
0.5
0
-0.5
0
50
100
150
b)
$\alpha_n(\theta)$ [degrees]
30
20
10
0
-10
0
50
100
150
c)
$U_n^*(\theta)$
3
2.5
2
1.5
1
0
50
100
150
θ [degrees]
ω Regulation
ω Regulation IQR
Q_c Regulation
Q_c Regulation IQR

ACCEPTED

This manuscript was accepted by Renewable Sustainable Energy. Click here to see the version of record.

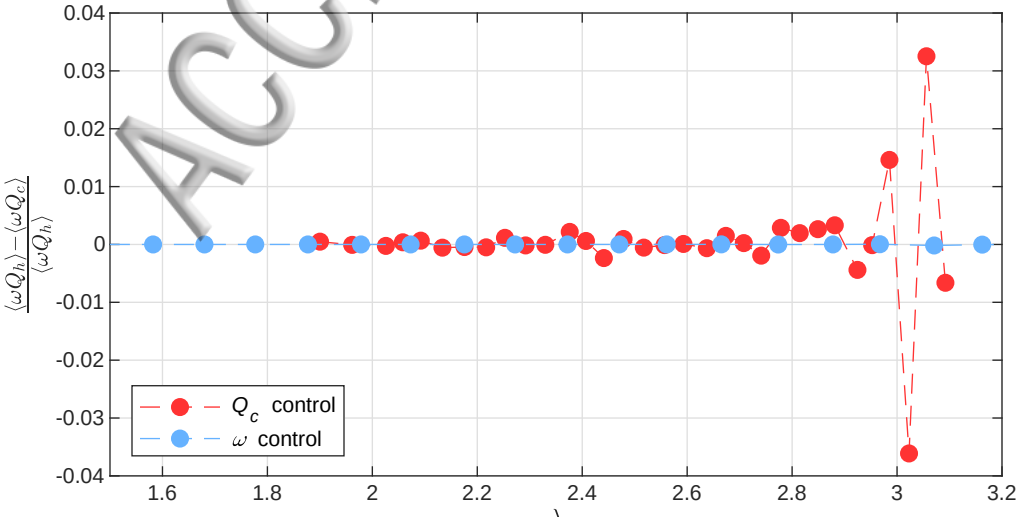
AIP Publishing

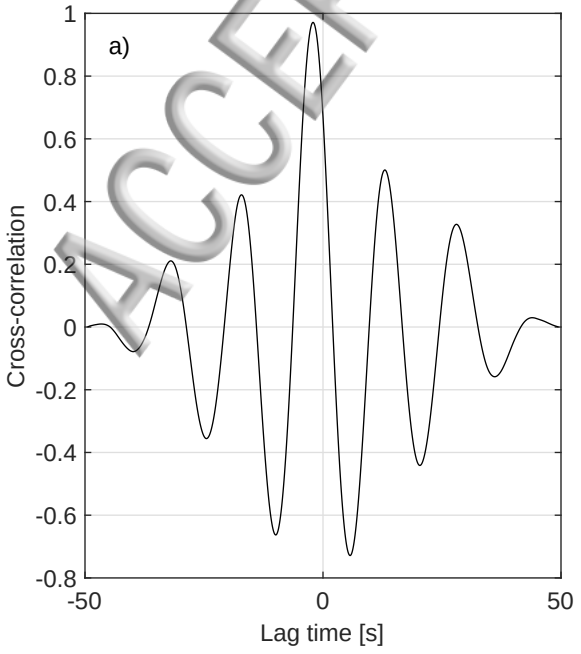
ACCEPTED MANUSCRIPT

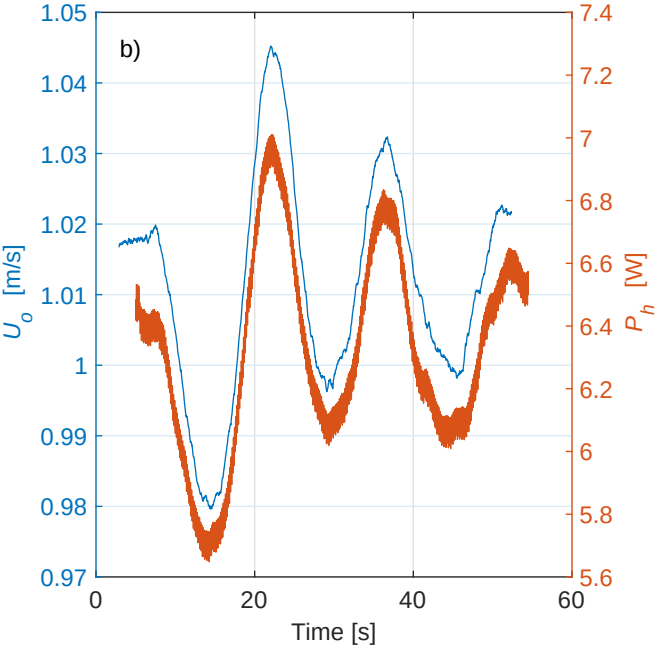


a) ω regulation

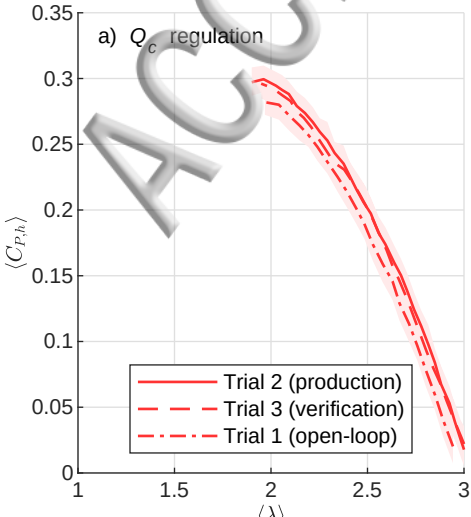
b) Q_c regulation

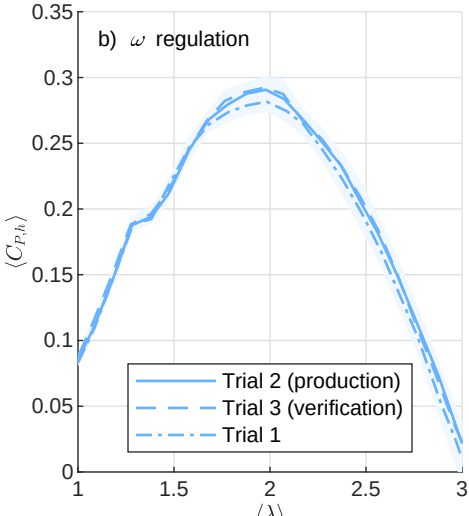

0.04
0.03
0.02
0.01
0
-0.01
-0.02
-0.03
-0.04
1.6
1.8
2
2.2
2.4
2.6
2.8
3
3.2
λ
$\frac{\langle \omega Q_h \rangle - \langle \omega Q_c \rangle}{\langle \omega Q_h \rangle}$
Q_c control
ω control
ACCE

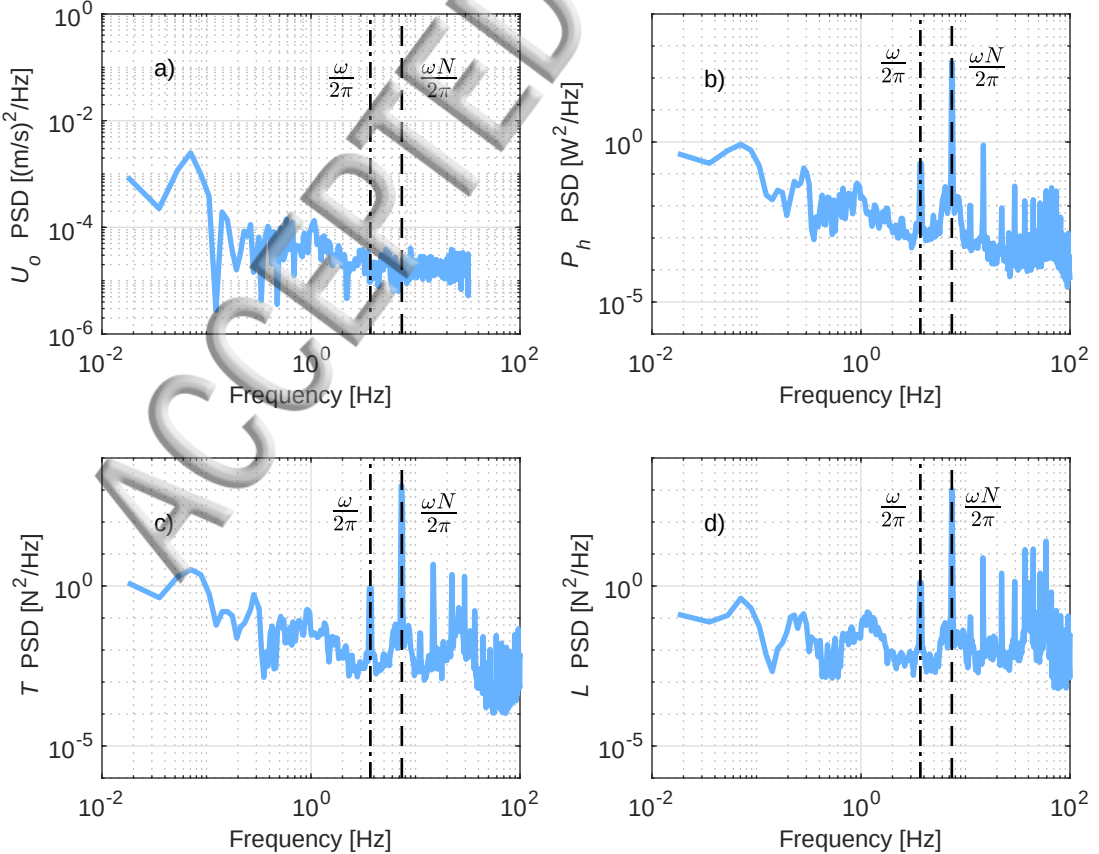

a)
Cross-correlation
Lag time [s]
1
0.8
0.6
0.4
0.2
0
-0.2
-0.4
-0.6
-0.8
-50
0
50


b)
U_o [m/s]
P_h [W]
Time [s]
1.05
1.04
1.03
1.02
1.01
1
0.99
0.98
0.97
7.4
7.2
7
6.8
6.6
6.4
6.2
6
5.8
5.6
0
20
40
60

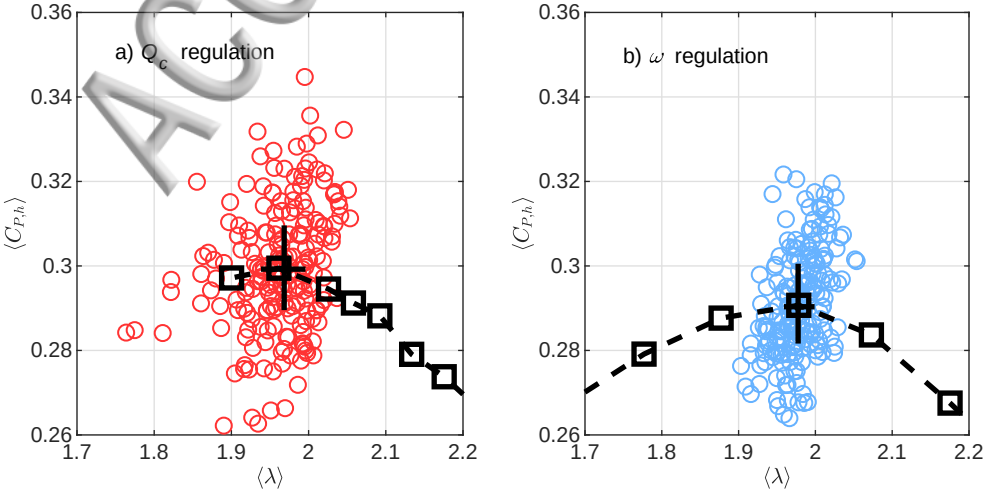
ACCEPTED


a) Q_c regulation
$\langle C_{P,h} \rangle$
$\langle \lambda \rangle$
0.35
0.3
0.25
0.2
0.15
0.1
0.05
0
1
1.5
2
2.5
3
Trial 2 (production)
Trial 3 (verification)
Trial 1 (open-loop)


b) ω regulation
$\langle C_{P,h} \rangle$
$\langle \lambda \rangle$
0.35
0.3
0.25
0.2
0.15
0.1
0.05
0
1
1.5
2
2.5
3
Trial 2 (production)
Trial 3 (verification)
Trial 1


a)
b)
c)
d)
$\frac{\omega}{2\pi}$
$\frac{\omega N}{2\pi}$
U_o PSD [(m/s)^2/Hz]
P_h PSD [W^2/Hz]
T PSD [N^2/Hz]
L PSD [N^2/Hz]
Frequency [Hz]
10^{-2}
10^{0}
10^{2}
10^{-6}
10^{-4}
10^{-2}
10^{0}
10^{-5}

ACCEPTED


a) Q_c regulation
b) ω regulation
$\langle C_{P,h} \rangle$
$\langle \lambda \rangle$
0.36
0.34
0.32
0.3
0.28
0.26
1.7
1.8
1.9
2
2.1
2.2